Nanocomplexes of Biodegradable Anticancer Macromolecules: Prolonged Plasma Half-life, Reduced Toxicity, and Increased Tumor Targeting

Jiayu Leong†, Joyce Tay†, Shengcai Yang, Chuan Yang, Eddy Wei Ping Tan, Yanming Wang, Bing Qian Tan, Sherwin Hor, Yau Hong Chua, Jeremy Pang Kern Tan, Qingfeng Chen, James L. Hedrick*, Yi Yan Yang*.

J. Leong, J. Tay, C. Yang, J. P. K. Tan, Y. Y. Yang

Bioprocessing Technology Institute (BTI), Agency for Science, Technology and Research (A*STAR), 20 Biopolis Way, Centros #06-01, Singapore 138668, Republic of Singapore

S. Yang, Y. Wang, B. Q. Tan, S. Hor, Y. H. Chua

Institute of Bioengineering and Bioimaging (IBB), Agency for Science, Technology and Research (A*STAR), 31 Biopolis Way, Nanos #07-01, Singapore 138669, Republic of Singapore

Email: yyyang@ibb.a-star.edu.sg

E. W. P. Tan

Bioinformatics Institute (BII), Agency for Science, Technology and Research (A*STAR), 30 Biopolis Street, Matrix #07-01, Singapore 138671, Republic of Singapore

Q. Chen

Institute of Molecular and Cell Biology, Agency for Science, Technology and Research (A*STAR), 61 Biopolis Drive, Proteos, Singapore 138673, Republic of Singapore

J. L. Hedrick

IBM Almaden Research Center, San Jose, CA 95120, USA

Email: hedrick@us.ibm.com

†JL and JT contributed to the study equally.

Abstract

Anticancer drug resistance is a large contributing factor to the global mortality rate of cancer patients. Anticancer macromolecules such as polymers were recently reported to overcome this issue. Anticancer macromolecules have unselective toxicity because they are highly positively charged. Herein, an anionic biodegradable polycarbonate carrier was synthesized and utilized to form nanocomplexes with an anticancer polycarbonate *via* self-assembly to neutralize its positive charges. Biotin was conjugated to the anionic carrier and served as a cancer cell-targeting moiety. The nanoparticles had sizes of <130nm with anticancer polymer loading levels of 38%-49%. Unlike the small molecular anticancer drug doxorubicin, the nanocomplexes effectively inhibited the growth of both drug-susceptible MCF7 and drug-resistant MCF7/ADR human breast cancer cell lines with low half maximal inhibitory concentration (IC_{50}). The nanocomplexes increased the anticancer polymer's *in vivo* half-life from 1h to 6 - 8h, and rapidly killed BT474 human breast cancer cells primarily *via* an apoptotic mechanism. The nanocomplexes significantly increased the median lethal dose (LD50) and reduced the injection site toxicity of the anticancer polymer. They suppressed tumor growth by 32% - 56% without causing any damage to the liver and kidneys. These nanocomplexes may potentially be used for cancer treatment to overcome drug resistance.

Keywords: polymeric nanocomplexes, polycarbonates, supramolecular assembly, anticancer macromolecule, drug-resistance

1. Introduction

Approximately 10 million deaths were caused by cancer and the number of new cases was estimated to be 19 million in 2020.[1] The survivability of cancer patients is largely dependent on their ability to respond to treatment such as chemotherapy. Cancer drug resistance is the primary cause of death in most advanced stage cancers[2] and is estimated to be the cause for 90% of treatment failures.[3] As a result, patients and their doctors often need to search for new cancer treatment options. However, the development of effective cancer treatments is often plagued with pharmacological challenges, which include the intrinsic drug resistance by the tumor cells[4] or the induction of resistance by the chemotherapy drug,[5] low drug solubility, insufficient drug accumulation in tumor tissue, rapid clearance from the body, and significant off-target toxicity. These issues motivated the extensive development of drug delivery systems to increase drug solubility, accumulation in tumor tissue and circulation half-life and to reduce the inherent drug toxicity. To date, more than 17 nanoparticle formulations for cancer therapy are in clinical trials and 8 have received United States Food and Drug Administration or European Medicines Agency approval for human use.[6] However, many of these drug delivery systems share the same limitations as the drug that they are carrying because the drug carrier does not change the mechanism of action of the drug. Therefore, there is a need for a different approach in the anticancer drug development.

Macromolecular therapeutics, which include peptides and synthetic polymers, are an emerging class of potential drugs that might overcome the problem of drug resistance.[7] This is because most of these macromolecules kill the target cells through physical disruption of cell membrane or by interacting with multiple proteins and/or genes within the cell. Compared to normal cells, cancer cell membrane has a net negative charge due to a greater abundance of anionic

biomolecules, such as phosphatidylserines, sialic acid residues and heparin sulfates.[8] Accordingly, peptides[9] or polymers[10] that effectively kill cancer cells contain lysine residues or quaternary ammonium groups that bind to the negatively charged cancer cells and hydrophobic residues that facilitate cell membrane disruption. There are a small number of peptides currently evaluated in clinical trials as anticancer agents.[11] On the other hand, cell-penetrating peptides[12] or polymers[13] that commonly consist arginine residues or guanidinium groups impose cytotoxicity by binding to intracellular components. For instance, cell-penetrating peptide p28, which is now in clinical trials, produces a post-translational increase in p53 in cancer cells by inhibiting its ubiquitination.[14] Importantly, cancer cells are unable to develop resistance towards these positively charged macromolecules after repeated use.[10]

Highly positively charged macromolecules (peptides or polymers) largely exist as individual chains in solution. With the positive charges unmasked, there is unselective toxicity when they bind by chance to healthy cells. As a result, many anticancer peptides and polymers have met with limited success. For example, the dose that can be injected would be limited by the maximum tolerable dose of the macromolecules and might not be suitable for intravenous injection. Instead, the macromolecules would have to be injected intratumorally.[15] On the other hand, those that self-assemble into higher order structures display better selectivity towards cancer cells over normal cells.[10, 13a, 16] However, in these nanoparticles, cationic charges from the anticancer polymers were not neutralized, which could limit their therapeutic window for clinical application.

Besides the overexpression of negatively charged biomolecules, cancer cells also overexpress cell surface receptors such as the sodium dependent multivitamin transporter to take up more nutrients to support their rapid proliferation. Biotin is a growth promoter of cells and is

translocated into cells to function as a coenzyme for carboxylase enzymes.[17] Therefore, biotin has been evaluated by several groups as a targeting moiety in cancer drug delivery.[18]

Polycarbonates are biodegradable polymers that have been designed as carriers for small molecule drug[19] and nucleic acid delivery.[20] The organocatalytic ring-opening polymerization (OROP) provides easy incorporation of a variety of functional groups with excellent biocompatibility and well-defined molecular length.[21] Here, we used OROP to synthesize negatively charged polycarbonate carriers and use them to neutralize the positive charges in the guanidinium-based anticancer polycarbonates through ionic interaction,[22] producing nanocomplexes (nanoparticles) through self-assembly for systemic delivery of the anticancer polymers (**Figure 1**). Specifically, we synthesized two types of anionic polycarbonates, a carboxylic acid-functionalized and a benzoic acid-functionalized polycarbonate. Additionally, biotin was conjugated on the anionic polymers to present itself on the surface of the nanoparticles after the self-assembly to increase its uptake by cancer cells. The pharmacokinetics and median lethal dose of polymers were evaluated *in vivo* to determine if the nanoparticles increased the anticancer polymer half-life and tolerable dose. The anticancer activity was also studied on breast cancer cell lines. Finally, the *in vivo* antitumor efficacy was evaluated in a human breast cancer xenograft mouse model, and *in vivo* toxicity was also examined.

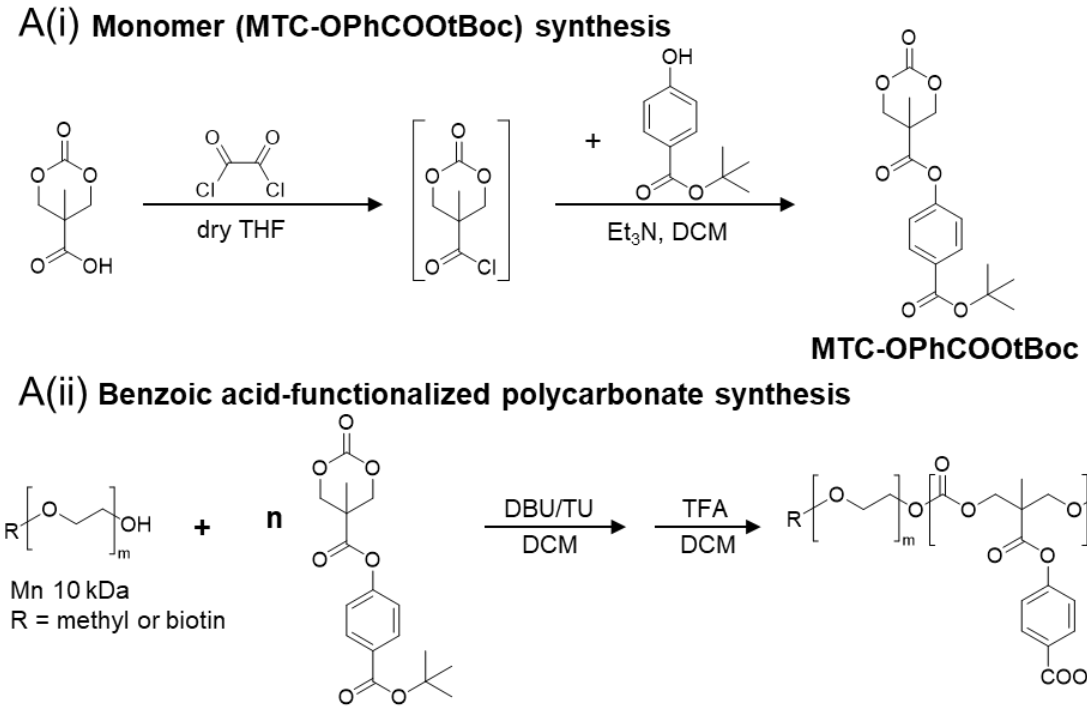
A(i) Monomer (MTC-OPhCOOtBoc) synthesis
dry THF
Et3N, DCM
MTC-OPhCOOtBoc
A(ii) Benzoic acid-functionalized polycarbonate synthesis
Mn 10 kDa
R = methyl or biotin
DBU/TU
DCM
TFA
DCM
COOH

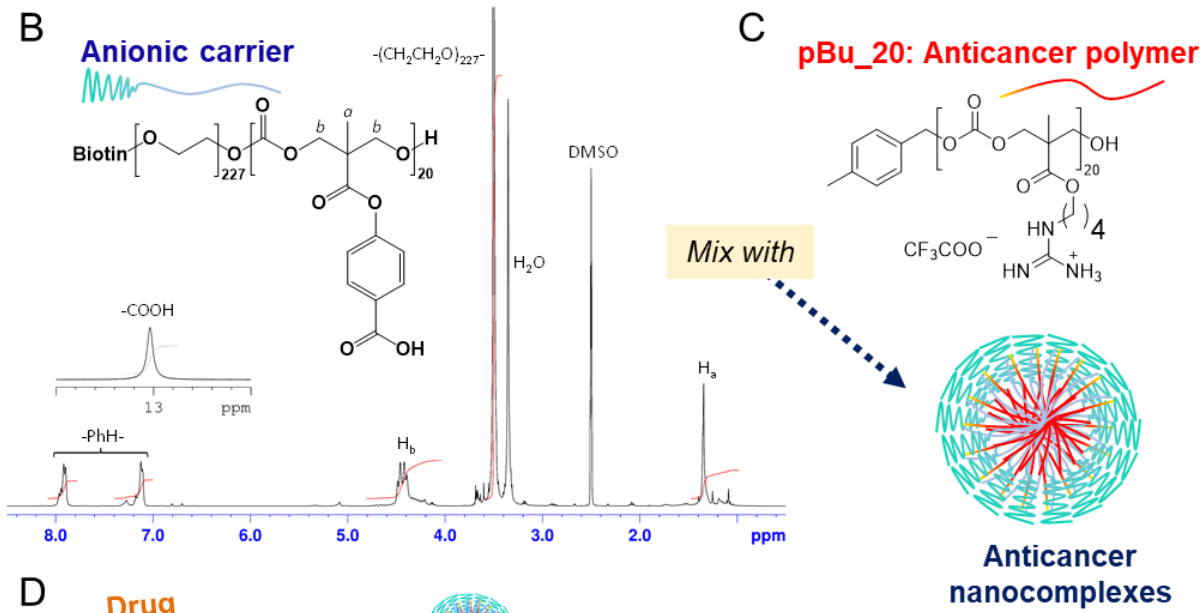
B
Anionic carrier
Biotin
-COOH
-PhH-
DMSO
H2O
Ha
Hb
8.0
7.0
6.0
5.0
4.0
3.0
2.0
ppm
C
pBu_20: Anticancer polymer
Mix with
Anticancer nanocomplexes

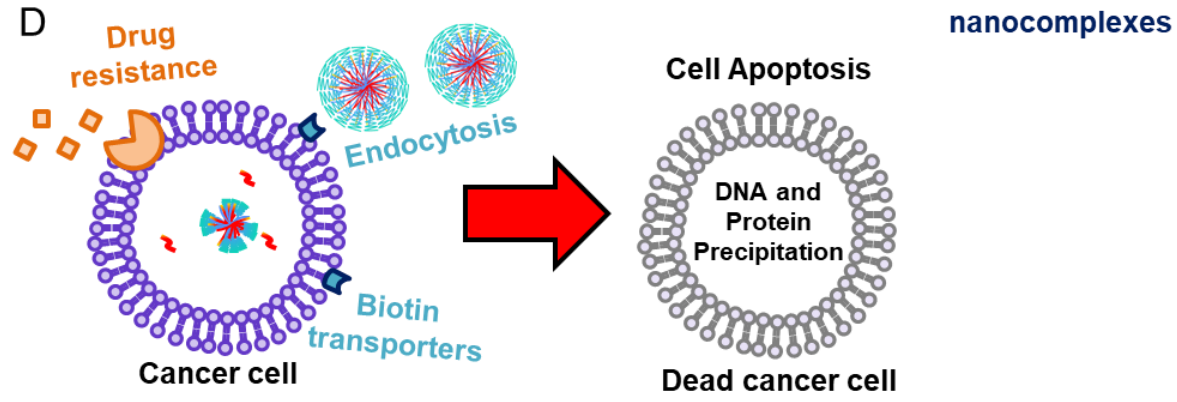
D
Drug resistance
Endocytosis
Biotin transporters
Cancer cell
Cell Apoptosis
DNA and Protein Precipitation
Dead cancer cell

Figure 1. Synthesis of the anionic polycarbonates, formation of the nanocomplexes and their anticancer activity. A) Synthetic scheme of benzoic acid-functionalized (i) monomer and (ii) block copolymers. B) ^{1}H NMR spectrum of bioin-PEG10k-p(MTC-PhCOOH)$_{20}$ in DMSO-d_6. C) Neutralization of positive charges in the anticancer cationic polycarbonate (pBu_20) using the anionic polycarbonates via self-assembly. D) Schematic of nanoparticles targeting drug-resistant cancer cells that overexpress biotin transporters. Upon endocytosis of nanoparticles, the released anticancer polycarbonate might interact with nucleic acids and/or proteins in the cell, which might induce apoptosis of cancer cells.

2. Results and Discussion

2.1. Synthesis of anionic polymeric carriers

Aliphatic carboxylic acid and benzoic acid-functionalized polycarbonates were synthesized via OROP and the degree of polymerization (DP) for all the polymers was 20. This was intended to match the DP of the anticancer guanidinium-functionalized polymer, pBu_20, which was synthesized as reported in our earlier publication.[21, 23] For the aliphatic carboxylic acid polymer, the cyclic monomer containing the protected carboxylic acid (MTC-tBAc) was synthesized as reported in the literature.[24] In order for the polymer to perform as a carrier, MTC-tBAc was polymerized with PEG or Biotin-PEG as macroinitiators in the presence of catalysts DBU and TU (**Figure 1**). Benzoic acid-functionalized diblock copolycarbonates were synthesized in a similar way via OROP of cyclic carbonate monomer with pendent tBoc-protected benzoic acid group (MTC-OPhCOOtBoc). GPC (gel permeation chromatography) results indicated that all the polymers exhibited narrow molecular weight distributions with low polydispersity indices ranging between 1.16 and 1.18 (**Figure S1**). The ^{1}H NMR results indicated that DP of all the polymers was 20. This was computed by referencing the integrated intensities of relevant resonances attributed from protons of PEG at 3.64 ppm with respect to hydrogens of the ethylene groups on the polycarbonate backbone at 4.45 ppm. Trifluoroacetic acid removed the tBoc protecting group in nearly quantitative yields. The complete deprotection was determined by the disappearance of the

methyl peak of the tBoc moieties in **Figure 1B**. Additionally, the DP of the polymer remained as 20, indicating there were no degradation of the polymer backbone during the deprotection step.

Estimated pKa from empirical calculations are 3.2 and 3.9 for the aliphatic carboxylic acid and benzoic acid, respectively (**Figure S2**). It was noted the pKa values are lower than the typical values for aliphatic carboxylic acid and benzoic acid, respectively because there is an electron-withdrawing ester group next to them. This implies that in a neutral pH buffer, both acids are deprotonated. As they move towards a more acidic environment, there will be more protonated benzoic acid than aliphatic carboxylic acid. This would affect the intermolecular electrostatic attraction to the guanidinium polymer where the benzoic acid has weaker attraction to the guanidinium group.

2.2. Formation of nanocomplexes from the anionic carrier and the cationic anticancer polycarbonate

When the carboxylic acid-functionalized polycarbonate was used as the carrier to form NP A, the self-assembly took place in aqueous solution by adding the anionic polymers to the cationic anticancer pBu_20 polymer. When the benzoic acid-functionalized polycarbonate was used as the carrier to form NP B, the simple mixing in aqueous solution was not possible because the benzoic acid-functionalized polycarbonate self-assembled before the addition of pBu_20. It was difficult to incorporate pBu_20 into the benzoic acid nanoparticles because it required interrupting the intermolecular bonds within the assembled nanoparticles. Therefore, a thin film hydration technique was used to create a thin film of the unassembled anionic polymer. Then, the anionic

and cationic polymer were immediately mixed when the film was hydrated with a solution of pBu_20.

The average hydrodynamic diameters for NP A were 38.5 nm and 33.8 nm for the mPEG and biotin-PEG anionic copolymers (**Table 1**). The nanoparticles were monodispersed in water with polydispersity indices of 0.09 to 0.11 and were overall neutrally charged with zeta potentials of 2 - 5 mV. On the other hand, the average hydrodynamic diameters for NP B were 123 nm and 120 nm for the mPEG and biotin-PEG anionic copolymers, respectively, and had zeta potentials of 15 - 17 mV. The slightly positive zeta potential was due to the higher loading of pBu_20. TEM images further demonstrated that the NP A_biotin PEG and NP B_biotin PEG were spherical in shape (**Figure S3**). The nanoparticles formed were stable over 3 h in PBS and BSA-containing PBS solution (80 g/L) (**Figure S4**).

Table 1. Hydrodynamic diameter, polydispersity index, zeta potential, loading level of nanoparticles loaded with pBu_20.

Nanoparticles	Anionic carrier	Diameter (nm)	Polydispersity index	Zeta Potential (mV)	Loading level (%)	Exposed biotin molecules (%)
NP A_mPEG	mPEG-p(MTC-$CH_2COOH)_{20}$	38.5 ± 0.7	0.09 ± 0.02	5 ± 3	38 ± 2	-
NP A_biotinPEG	biotin-PEG-p(MTC-$CH_2COOH)_{20}$	33.8 ± 0.8	0.11 ± 0.02	2 ± 1	38 ± 3	41 ± 2
NP B_mPEG	mPEG-p(MTC-$PhCOOH)_{20}$	123 ± 11	0.21 ± 0.02	15 ± 3	44 ± 7	-
NP B_biotinPEG	biotin-PEG-p(MTC-$PhCOOH)_{20}$	120 ± 13	0.13 ± 0.03	17 ± 5	49 ± 5	44 ± 3

To determine the loading level of pBu_20 in the nanoparticles, we used a ligand-exchange guanidine assay.[36, 37] The loading level of pBu_20 in NP A was 38% for both the mPEG and biotin-PEG anionic copolymers (**Table 1**). The loading level of pBu_20 in NP B was 44% and 49% for the mPEG and biotin-PEG anionic copolymers, respectively. The number of biotin molecules was also determined to confirm that the biotin moiety is accessible after the nanoparticles were formed. The percentage of biotin molecules that was exposed was 41% and 44% for NP A and NP B, respectively.

2.3. *In vitro* cytotoxicity of pBu_20 loaded nanoparticles

The anticancer activity of pBu_20 loaded nanoparticles was determined using a metabolic activity assay to determine the half maximal inhibitory concentration (IC_{50}) on human breast cancer cell lines, BT474, MCF7 and doxorubicin-resistant MCF7 (MCF7/ADR). Live cells reduced the non-fluorescent resazurin dye to fluorescent resorufin. The IC_{50} for doxorubicin against BT474 was 4 µg/mL. The anticancer polymer pBu_20, and encapsulated pBu_20 in NP B_mPEG and NP B_biotinPEG had slightly higher IC_{50} values, which were 13.6 µg/mL, 34.4 µg/mL and 25.0 µg/mL, respectively (**Figure 2**). In contrast, IC_{50} values for encapsulated pBu_20 in NP A_mPEG and NP A_biotinPEG were significantly higher, which were 135 µg/mL and 1002 µg/mL, respectively (**Figure S5**). The decrease in potency in biotinylated NP_A as compared to its non-biotinylated counterpart could be attributed to the formation of strong intramolecular hydrogen bonding between the carboxylic acid group and urea group on the biotin and thus, protonation of the carboxylic acid groups in biotinylated NP_A might be more difficult to dissociate the nanoparticles as compared to the non-biotinylated form, thereby hampering the release of pBu_20. Nevertheless, further investigation is needed to understand reasons behind the

decrease in potency in biotinylated NP_A as compared to its non-biotinylated counterpart. The greater cellular uptake of NP B_biotinPEG as compared to NP A_biotonPEG (Figure S6) might be a reason for the stronger anticancer activity. A decomplexation assay was performed using triton X-100 to compare the binding between the carboxylic acid group and the guanidinium group in NP A_bioPEG and NP B_biotinPEG (Figure S7). The results showed that the decomplexation of NP A_biotinPEG (reduction in the intensity of nanoparticles in solution by dynamic light scattering-DLS) occurred after 1 h of incubation. In contrast, the decomplexation of NP B_biotinPEG began shortly after 5 min of incubation. Triton X-100 was able to act on NP B_biotinPEG more readily as compared to NP A_biotinPEG to cause dispersion of the nanoparticles, and this might be another reason for the stronger anticancer activity of NP B_biotinPEG. These results indicate that NP B could release pBu_20 from the endosomes into the cytosol readily where it could interact with intracellular proteins and nucleic acids, leading to cell death.[13b] However, NP A might not release pBu_20 effectively from the endosomes possibly due to stronger electrostatic interactions between the carboxylic acid group and the guanidinium group as the aliphatic carboxylic acid groups in NP A with lower pKa might be less readily protonated in the endosomes to release the anticancer polymer as compared to the benzoic acid groups in NP B (**Figure S2**).

When tested against MCF7 and MCF7/ADR, doxorubicin was ineffective against MCF7/ADR as compared to MCF7 (IC_{50}: 0.62 μg/mL *vs.* >100 μg/mL) due to resistance in MCF7/ADR. The anticancer macromolecule pBu_20 and its nanoparticle formulations (NP B_mPEG and NP B_biotinPEG) were similarly effective against both MCF7 and MCF7/ADR cells (**Figure 2**), indicating that MCF7/ADR cells were not resistant towards pBu_20 or its nanoparticle formulations. In addition, pBu_20 and its nanoparticle formulations had stronger

activity against MCF7/ADR with lower IC_{50} values than doxorubicin. This phenomenon was similar to that observed previously for other anticancer polymers, whereby the anticancer polymers were successful in killing drug-resistant cancer cells as compared to the small molecular anticancer drug doxorubicin.[10, 13a, 26] Furthermore, the biodegradable polycarbonate-based nanoparticles reported in this study would be less susceptible to proteolytic cleavage as compared to previously reported polypeptide-based anticancer nanoparticles.[27] From **Figure 2B**, pBu_20 and doxorubicin had low or no selectivity towards cancer cells over healthy HK2 cells, while both nanoparticle formulations had significantly higher selectivity towards the cancer cells as evidenced by their lower IC_{50} values against cancer cells as compared to HK2 cells. As such, our findings demonstrated that these nanoparticles represent safe and effective antineoplastic agents, which shed new light on the development of drug-free synthetic polymers for cancer therapy. Since NP B were more efficacious than NP A, the subsequent studies were focused on the former.

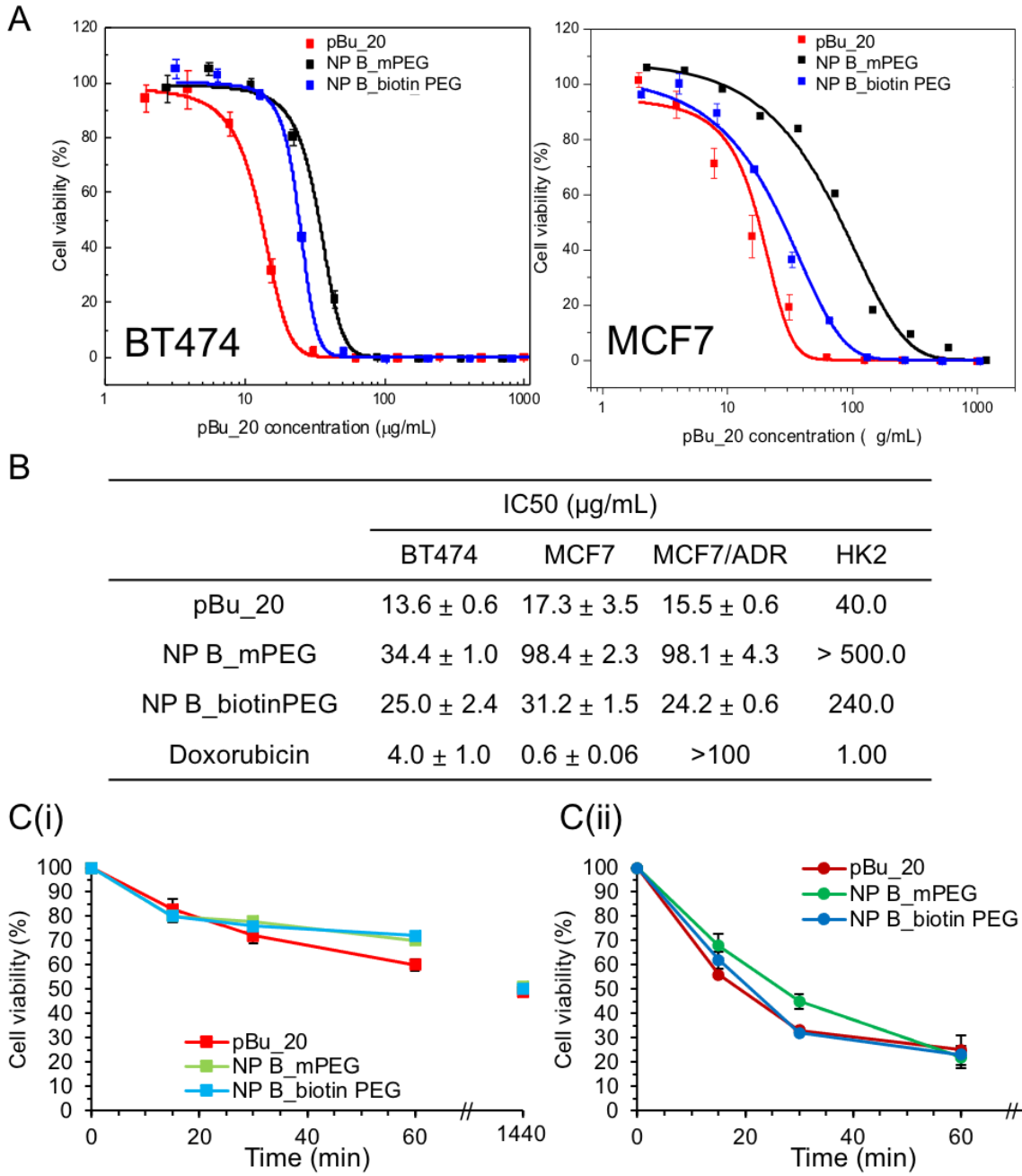

B

	IC50 (μg/mL)			
	BT474	MCF7	MCF7/ADR	HK2
pBu_20	13.6 ± 0.6	17.3 ± 3.5	15.5 ± 0.6	40.0
NP B_mPEG	34.4 ± 1.0	98.4 ± 2.3	98.1 ± 4.3	> 500.0
NP B_biotinPEG	25.0 ± 2.4	31.2 ± 1.5	24.2 ± 0.6	240.0
Doxorubicin	4.0 ± 1.0	0.6 ± 0.06	>100	1.00

Figure 2. *In vitro* cytotoxicity of pBu_20 and its nanoparticle formulations against BT474, MCF7, doxorubicin-resistant MCF7/ADR cancer cell lines as well as HK2 healthy cell line. A) Cytotoxicity of pBu_20 at concentrations ranging from 2 to 1000 μg/mL after incubation with the cells for 24 h. B) Summary of the half maximal inhibitory concentrations. C) Killing kinetics of pBu_20 and its nanoparticle formulations at (i) IC_{50} and (ii) $2\times IC_{50}$ against MCF7 cells. Values represent mean ± standard deviation (n=4).

The killing kinetics of pBu_20 and its nanoparticle formulations were studied at IC_{50} and $2\times IC_{50}$ against MCF7 cells (**Figure 2C**). At IC_{50}, both NP B_mPEG and NP B_biotinPEG reduced the number of viable cells to 70%, whereas pBu_20 reduced the number of viable cells to 60% within 60 min. At $2\times IC_{50}$, pBu_20, NP B_mPEG and NP B_biotinPEG reduced the number of viable cells to 25% within 60 min. These findings demonstrated that pBu_20 and its nanoparticle formulations killed the cancer cells rapidly.

2.4. Exploration of anticancer mechanism

The intracellular distributions of pBu_20 and its nanoparticle formulations were first studied by conjugating pBu_20 with Alexa Fluor 488 dye and viewing the cells using a confocal laser scanning microscope. **Figure 3A** shows the cells after 2 h of treatment with pBu_20, NP B_mPEG and NP B_biotin PEG at IC_{50}. The polymer is colored green and acidic organelles such as the endolysosomes are stained red. For cells that were treated with pBu_20, there was little co-localization of the polymer and the acidic organelles (i.e. few yellow regions only), indicating that pBu_20 entered the cells likely via membrane translocation.[28] In contrast, for the cells that were treated with the nanoparticle formulations, there were many yellow regions, implying that the nanoparticles were co-localized with the endolysosomes after being taken up by the cells via endocytosis. This finding is in agreement with other nanoparticles reported in the literature. [19d, 19e, 29]

In addition, to confirm that cytotoxicity is a result of endocytosis of the nanoparticles, the entry pathway was blocked with chlorpromazine inhibitor. BT-474 cells were pre-treated with 5 μg/mL of chlorpromazine and incubated for 2 h prior to the 2 h-treatment with pBu_20, NP

B_biotinPEG and NP B_mPEG. The IC_{50} values for pBu_20, NP B_mPEG and NP B_biotinPEG and obtained were 130.0 μg/mL, 402.0 μg/mL and >1000 μg/mL, respectively (**Figure S8**). The IC_{50} values of NP B_mPEG and NP B_biotinPEG obtained from chlorpromazine pre-treated cells were much higher than the IC_{50} values obtained without chlorpromazine pre-treatment, which were 120 μg/mL and 40.0 μg/mL, respectively. Clearly, chlorpromazine did not affect the uptake of the free polymer pBu_20 by BT474 cells significantly (IC_{50}: 130.0 *vs.* 180.0 μg/mL), while it significantly suppressed the cellular uptake of the nanoparticles by blocking the entry pathway into the cells and prevented cell death, thereby resulting in significantly higher IC_{50} values. Interestingly, the chlorpromazine blocking effect was more significant against the endocytosis of NP B_biotinPEG than that of NP B_mPEG. These results further confirmed the observation from confocal imaging that the uptake of the nanoparticles was mainly *via* endocytosis.

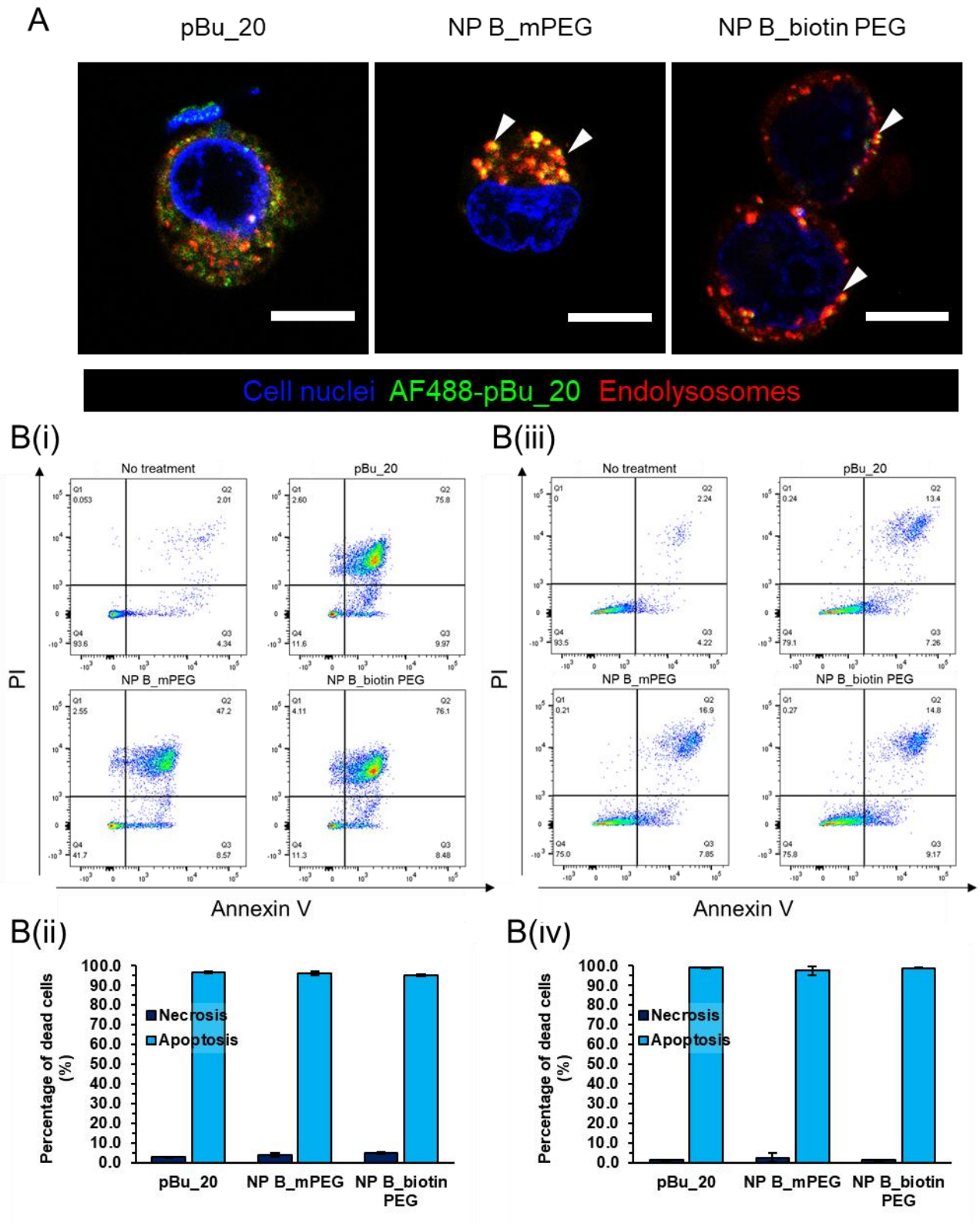
A
pBu_20
NP B_mPEG
NP B_biotin PEG
Cell nuclei AF488-pBu_20 Endolysosomes
B(i)
No treatment
pBu_20
NP B_mPEG
NP B_biotin PEG
PI
Annexin V
B(iii)
No treatment
pBu_20
NP B_mPEG
NP B_biotin PEG
PI
Annexin V
B(ii)
Percentage of dead cells (%)
Necrosis
Apoptosis
pBu_20
NP B_mPEG
NP B_biotin PEG
B(iv)
Percentage of dead cells (%)
Necrosis
Apoptosis
pBu_20
NP B_mPEG
NP B_biotin PEG

Figure 3. Exploration of anticancer mechanism. A) Intracellular distribution of pBu_20, NP B_mPEG and NP B_biotinPEG. pBu_20 was conjugated with AF488 dye before forming the nanoparticles with the anionic polymers. The cells were incubated with pBu_20 or its nanoparticles for 30 min at 37 °C before the nuclei and endolysosomes were stained blue and red, respectively. Images were taken at 2 h after the polymer or nanoparticles were added. Scale bar represents 10 µm. The arrows pointing to the yellow regions. B) Apoptotic cell population after 2 h of incubation with pBu_20 or its nanoparticle formulations at different concentrations. (i) and (ii) BT474 cells; pBu_20 concentrations: 30 µg/mL, 100 µg/mL and 50 µg/mL for pBu_20, Nanoparticles B_mPEG and Nanoparticles B_biotinPEG, respectively. Values represent mean ± standard deviation (n=3). (iii) and (iv) MCF7 cells; pBu_20 concentrations: 17 µg/mL, 100 µg/mL and 25 µg/mL for pBu_20, Nanoparticles B_mPEG and Nanoparticles B_biotinPEG, respectively. Values represent mean ± standard deviation (n=3). Apoptotic cells were stained with Alexa Fluor 488-conjugated annexin V and dead cells were stained with propidium iodide (PI). Annexin $V^{Low}PI^{Low}$: live cells; Annexin $V^{High}PI^{Low}$: early apoptotic cells; Annexin $V^{High}PI^{High}$: late apoptotic cells; Annexin $V^{Low}PI^{High}$: necrotic cells.

Next, we investigated if the cells died through apoptosis or necrosis. To do so, the cells were treated with pBu_20 or its nanoparticle formulations for 2 h at their respective IC_{50}. Then, they were incubated with a mixture of recombinant annexin V, Alexa Fluor 488-conjugated pBu_20 and nanoparticles, and propidium iodide (PI). The recombinant annexin V binds to cells that present phosphatidylserine on the external surface of the cell membrane. High level of externalized phosphatidylserine is an indicator for apoptosis. On the other hand, PI enters and stains cells that have damaged membranes, which is an indicator for necrosis. Cells that were treated with pBu_20 or its nanoparticle formulations elevated the population of early apoptotic cells (1.7 – 2.2-fold increase compared to the control group without any treatment) and negligible levels of PI (less than 4.11% for BT474 and 0.27% for MCF7) (**Figure 3B**). This suggested that the anticancer mechanism is primarily based on apoptosis, regardless of whether pBu_20 was delivered to the cells as a free polymer or in nanoparticles. These findings are marked contrast to the findings of quaternary ammonium-functionalized nanoparticles, where the nanoparticles induced necrosis in cancer cells due to membrane disruptive activity of quaternary ammonium-functionalized nanoparticles.[10]

Pharmacokinetics of the nanoparticles

To determine if the formation of nanoparticles would increase the retention time of pBu_20 in the body, the amount of pBu_20 in the blood plasma and the major organs were measured (**Table S1-S4**). In a previous study, the half-life of pBu_20 in mice was 59 min after intravenous injection.[30] By complexing with the anionic copolymers to form nanoparticles, the half-life of pBu_20 increased by 4 – 9-folds (**Table 2**). The half-life of pBu_20 was increased to 440 min and 529 min when mPEG and biotinPEG carboxylic acid-functionalized polycarbonates were used as the carriers to form NP A_mPEG and NP A_biotinPEG, respectively. There was no significant difference between the 2 types of nanoparticles. The half-life of pBu_20 was also significantly prolonged when it was delivered by the benzoic acid-functionalized polycarbonates (59 min *vs.* 390 and 252 min for NP B_mPEG and NP B_biotinPEG, respectively).

Table 2. Plasma half-life of pBu_20 and pBu_20-loaded nanoparticles.

Polymer/Nanoparticles	Half-life (min)
pBu_20	59*
NP A_mPEG	440 ± 113
NP A_biotinPEG	529 ± 100
NP B_mPEG	390 ± 16
NP B_biotinPEG	252 ± 71

* Taken from Reference [30].

The distribution of pBu_20 to the major organs at each time point was determined by measuring the fluorescence intensity of the dye-conjugated pBu_20 polymer in the major organs

(e.g. brain, heart, kidneys, liver, lungs, and spleen). There were about 10-folds higher levels of pBu_20 in the liver and kidneys compared to the spleen and lungs (**Figure S9**). The highest polymer concentration was at 2 min and the polymer concentration decreased over time. After 24 h, the amount of pBu_20 in the organs was below the detection limit for NP A. On the other hand, there were still about 10% detected in the liver and spleen for NP B. For NP A and NP_B, the amount of the pBu_20 in the brain and heart at all time points was below the detection limit.

In vivo antitumor efficacy and toxicity evaluation

To test if the pBu_20 nanoparticles could kill the tumor cells *in vivo*, the nanoparticles were administrated to nude mice bearing BT474 human breast cancer by intravenous injection. As the nanoparticles were below 200 nm and were stable in the presence of serum proteins (**Figure S4**), we took advantage of the fenestrated blood vessels formed by the tumors and injected the nanocomplexes intravenously. The mice were injected twice weekly for two weeks to give a total of four doses, which were each less than 30% of the LD_{50} to avoid toxicity (**Table S5**). The tumors on mice that were not given any treatment grew consistently and the volume tripled over the three weeks of observation (**Figure 4A**).

Among all formulations tested, NP B_biotinPEG at 20 mg pBu_20/kg of mouse body weight suppressed tumor growth effectively, and the average tumor size of the mice treated with NP B_biotinPEG at 20 mg pBu_20/kg of mouse body weight was significantly smaller than that of the untreated mice on day 21 (**Figure 4A**). There was no significant difference in the tumor volume among the treated groups. For mice that were injected with the free polymer pBu_20 at a dose of 8 mg/kg, significant injection site toxicity was noticed where the tails turned black and necrotic after 2 doses. The sudden drop in tumor volume of the pBu_20 treated group on day 21

was due to the death of mice with larger tumors. Additionally, a 16% lower body weight of the pBu_20 treated group than the untreated mice was observed on day 21 (**Figure 4B**). In the mice that were treated with NP B_mPEG at 8 mg pBu_20/kg of mouse body weight, no injection site toxicity and no drop in body weight were observed. The similar phenomena were seen in most of the mice (9 out of 10) treated with NP B_mPEG at 20 mg pBu_20/kg of mouse body weight. Seventy percent of the mice treated with NP B_biotinPEG at 20 mg pBu_20/kg of mouse body weight experienced injection site toxicity after the 3rd dose. However, it was observed that the injection site side-reaction was mitigated when the nanoparticle formulation was given in separate injections, indicating that i.v. infusion would be a better option to deliver the nanoparticle formulation in future clinical applications. There was no systemic toxicity in mice treated with nanoparticles as demonstrated by the constant body weight (**Figure 4B**).

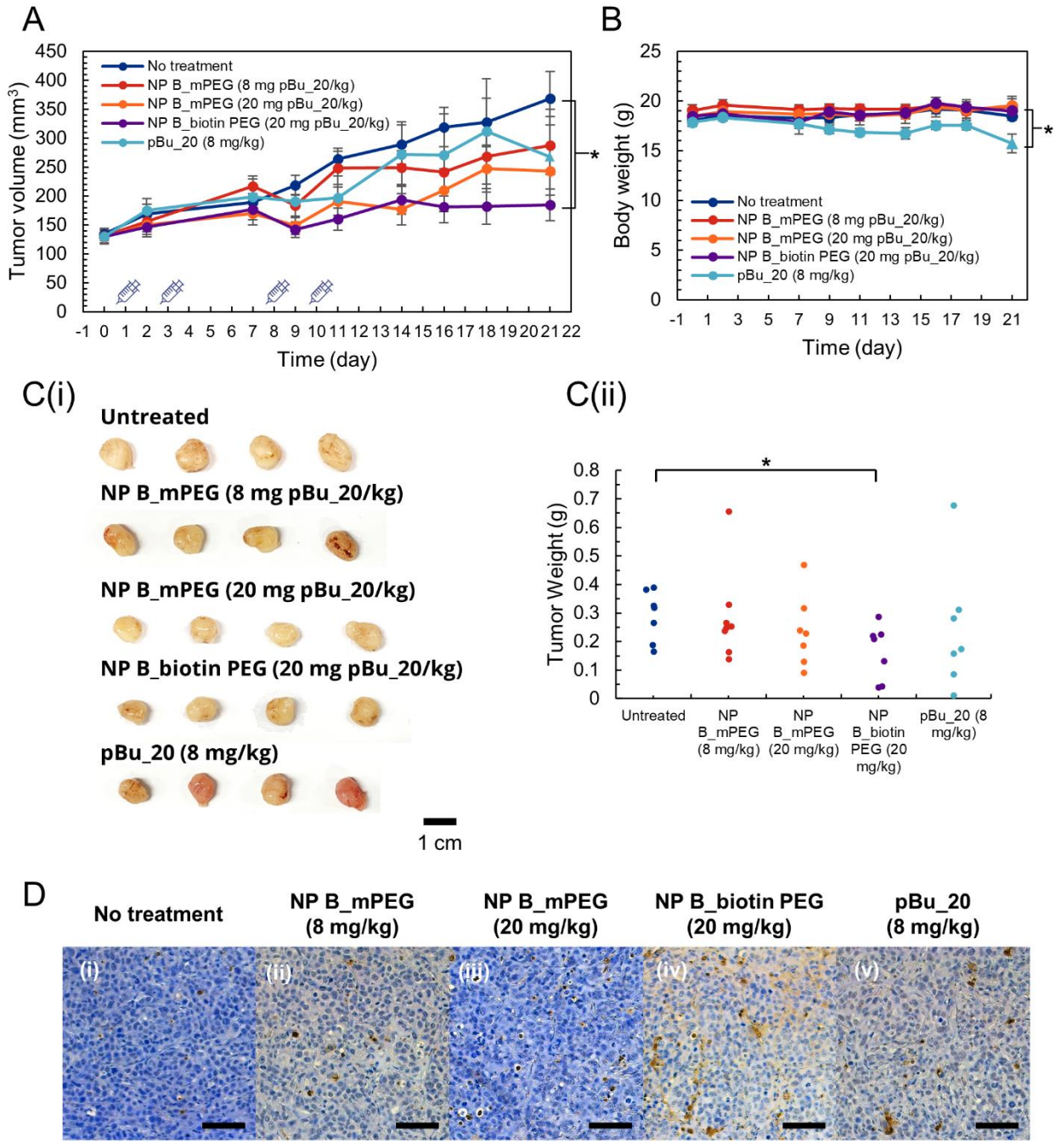

Figure 4. *In vivo* anticancer efficacy and mouse body weight changes over time after various treatments. A) Tumor volume and B) body weight measured over 20 days after the day of injection. Mice were injected with NP B_mPEG (8 or 20 mg pBu_20/kg), NP B_biotinPEG (20 mg pBu_20/kg) and pBu_20 (8 mg/kg) on day 1, day 3, day 8 and day 10. Values represent mean ± standard error (n = 7-9). The lines indicate significant difference between the groups by Student's t-test. *$p<0.05$. C) (i) Photographs of the middle four tumors when arranged in ascending order of tumor weight and (ii) weight measurement of tumors harvested on day 21. Values represent mean

± standard error (n = 7-9). The lines indicate significant difference between the groups by Student's t-test. *p<0.05. D) Tumors harvested at 20 days after the first injection were stained for apoptotic cells. Scale bar represents 100 μm.

On day 21, the tumors were harvested and weighed (**Figure 4C**). Consistent with the tumor volume measurements, the untreated control group had the heaviest average tumor weight of 0.34 g. However, the mice that were treated with NP B_biotin PEG with dose of 20 mg/kg had 43% tumor suppression as compared to the untreated group. There was no significant difference in the tumor weight between the untreated group and the groups treated with the rest nanoparticle formulations without biotin.

The tumors were studied by taking cross-sectional slices and staining them by the terminal deoxynucleotidyl transferase dUTP nick end labeling (TUNEL) assay which stains apoptotic cells (**Figure 4D(i) to (v)**). From the TUNEL assay, the cells in the treated tumors were spaced less compactly than those in the control tumor without treatment. In addition, there were more cells that were stained brown in the treatment groups, which indicated a higher number of apoptotic cells. The observation of apoptotic cancer cells was in agreement with *in vitro* flow cytometric study (**Figure 3B**).

The effect of the 4 doses of treatments on the liver were evaluated by H&E histology of the liver tissues, and no pathological abnormalities were observed (**Figure 5A**). The liver and kidney health statuses were also evaluated through serum biochemical tests. The serum of the treated mice had normal levels of urea and liver enzymes alanine transaminase and aspartate transaminase (**Figure 5B**).

A

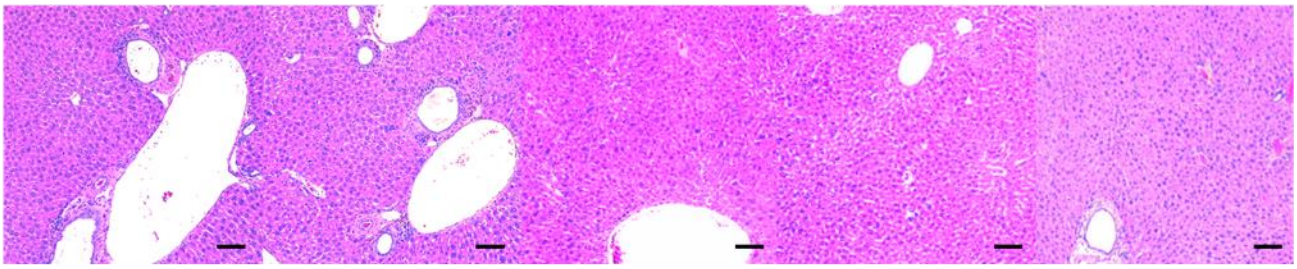

B

Treatment groups	BUN (mg/dL)	ALT (U/L)	AST (U/L)
NP B_mPEG (8 mg pBu_20/kg)	9 ± 3	51 ± 4	112 ± 44
NP B_mPEG (20 mg pBu_20/kg)	7 ± 2	42 ± 5	87 ± 5
NP B_biotin PEG (20 mg pBu_20/kg)	8 ± 3	47 ± 1	91 ± 11
pBu_20 (8 mg/kg)	11 ± 8	50 ± 10	109 ± 18
Normal range	6.07 - 13.5	28 - 132	59 - 247

Figure 5. Evaluation of *in vivo* toxicity. A) Liver tissues were harvested 20 days after the first injection of treatments. The tissues were fixed, embedded in paraffin, sectioned, and stained with hematoxylin and eosin. Scale bar represents 100 µm. B) Serum analysis for markers of kidney (blood urea nitrogen, BUN) and liver (alanine transaminase, ALT and aspartate transaminase, AST) health statuses. Values represent mean ± standard deviation (n = 3).

3. Conclusion

We have synthesized anionic polymers, which were functionalized with carboxylic acid or benzoic acid, and successfully used the polymers to form nanocomplexes with the anticancer polymer pBu_20 *via* self-assembly. The nanoparticles formed were below 200 nm. The formation of the nanoparticles neutralized the positive charges, increased the *in vivo* half-life and the LD50 of pBu_20. NP A formed from the aliphatic carboxylic acid-functionalized polycarbonate did not exert strong anticancer activity, while NP B formed from the benzoic acid-functionalized polycarbonate especially the one with biotin (NP B_biotin PEG) showed comparable anticancer activity as the free anticancer polymer pBu_20. Unlike doxorubicin, the nanoparticles were

effective in inhibiting the growth of drug-resistant MCF7/ADR. These nanoparticles were internalized by cells *via* endocytosis and killed the cancer cells primarily through apoptosis. In a BT474 human breast tumor xenograft mouse model, NP B_biotin PEG effectively suppressed the tumor growth without causing body weight loss or damage to the major organs. These nanoparticles have a potential use as an anticancer therapy to overcome drug resistance.

4. Experimental Section

Materials: Reagents were purchased from Sigma-Aldrich and used as received unless otherwise noted. 1,8-Diazabicyclo[5.4.0]undec-7-ene (DBU; 98%) was stirred over CaH_2, vacuum distilled twice, and then stored in a glove box. The cyclic carbonate monomer 5-methyl-2-oxo-1,3-dioxane-5-carboxylic acid (MTC-OH)[31] and *N*-(3,5-trifluoromethyl)phenyl-*N*'-cyclohexylthiourea (TU)[32] were prepared according to our previous protocols. They were freeze-dried under high vacuum before being transferred to the glove box.

Synthesis of benzoic acid-functionalized carbonate monomer (MTC-OPhCOOtBoc): MTC-OPhCOOtBoc was synthesized with reference to the protocol reported in our previous work (**Scheme S1**).[31] Briefly, in a dry three-neck round bottom flask, MTC-OH (4.35 g, 27.18 mmol) was dissolved in dry THF (50 mL), followed by adding several drops of DMF. A solution of oxalyl chloride (4.32 mL, 50 mmol) in dry THF (50 mL) was subsequently added dropwise under N_2 atmosphere. After the reaction solution was stirred for 1 h, the volatiles were removed by N_2 gas flow and under high vacuum sequentially, yielding the intermediate product MTC-Cl (5-methyl-2-oxo-1,3-dioxane-5-carbonyl chloride) as off-white solid. The solid was heated to 62 °C for a brief 2–3 min to remove unreacted oxalyl chloride, and then cooled down to room temperature and re-dissolved in dry DCM (50 mL). A solution of tert-butyl 4-hydroxybenzoate (4.85 g, 25 mmol) and triethylamine (6.89 mL, 49 mmol) dissolved in dry DCM (50 mL) was dropped over a duration of 30 min and the reaction mixture was allowed to react overnight before being transferred to a 1 L of separation funnel. After 200 mL of DCM was added, the solution was washed with brine (50 mL) for 3 times, and then dried over $MgSO_4$ overnight. Finally, after removal of solvent, the crude product was subjected to purification by flash column chromatography using silica gel and a hexane-ethyl acetate solvent system as the eluent to yield MTC-OPhCOOtBoc as white solid (83%

yield). ^{1}H NMR (400 MHz, $CDCl_3$, 22 °C): δ 8.01 (dd, 2H, -Ph*H*-), 7.12 (dd, 2H, -Ph*H*-), 4.83 (dd, 2H, -C*H*$_2$OCOO-), 4.32 (dd, 2H, -C*H*$_2$OCOO-), 1.57 (s, 9H, -CH_3 of tBoc), 1.32 (s, 3H, -CH_3).

Synthesis of benzoic acid-functionalized polycarbonate Biotin-PEG$_{10K}$-P(MTC-PhCOOtBoc)$_{20}$ (Scheme S2): Briefly, in a glovebox, Biotin-PEG-OH (M_n 10 kDa, 0.3 g, 0.03 mmol), MTC-OPhCOOtBoc (0.278 g, 0.825 mmol) and TU (6.11 mg, 0.0165 mmol) were dissolved in 2 mL of dry DCM in a 20 mL of vial, followed by addition of DBU (2.5 μL, 0.0165 mmol) to initiate the polymerization. After reacted for 2 h, about 2-3 mg of benzoic acid was added to quench the polymerization. Finally, the reaction solution was dropped on a Sephadex LH-20 column and purified by size exclusion chromatography (SEC) using THF as the eluent. After the solvent was removed, the residue was dried *in vacuo*, giving Biotin-PEG$_{10K}$-P(MTC-PhCOOtBoc)$_{20}$ as white solid (89% yield). PDI: 1.18. ^{1}H NMR (400 MHz, $CDCl_3$, 22 °C): δ 7.97 (dd, 40H, -Ph*H*-), 7.08 (dd, 40H, -Ph*H*-), 4.45 (m, 80H, -C*H*$_2$OCOO-), 3.64 (s, 909H, H of PEG), 1.56 (s, 180H, -CH_3 of tBoc), 1.32 (m, 60H, -CH_3).

Deprotection of tBoc-protected Biotin-PEG$_{10k}$-P(MTC-PhCOOtBoc)$_{20}$: For removal of tBoc protecting groups, an acid-mediated deprotection strategy was adopted. Briefly, the above tBoc-protected polymer (0.45 g) was dissolved in dry DCM (10 mL) and trifluoroacetic acid (10 mL). The reaction mixture was sealed and stirred at room temperature overnight. After the removal of solvent, the residue was re-dissolved in MeOH (2 mL) and precipitated in Et_2O. After the precipitate was centrifuged and washed with Et_2O for 3 times, the solid obtained was dried *in vacuo*, giving pure Biotin-PEG$_{10K}$-P(MTC-PhCOOH)$_{20}$ as white solid (93% yield). Complete deprotection was ascertained by ^{1}H NMR analysis. ^{1}H NMR (400 MHz, DMSO-d_6, 22 °C): δ 13.03

(s, br, 20H, -COO*H*), 7.90 (m, 40H, -Ph*H*-), 7.12 (m, 40H, -Ph*H*-), 4.44 (m, 80H, -C*H*$_2$OCOO-), 3.50 (s, 909H, H of PEG), 1.34 (m, 60H, -CH$_3$).

Synthesis of benzoic acid-functionalized polycarbonate PEG$_{10K}$-P(MTC-PhCOOH)$_{20}$: mPEG (10 kDa) was used as the macro-initiator according to the protocol described for the synthesis of Biotin-PEG$_{10K}$-P(MTC-PhCOOH)$_{20}$. Yield: 92%; PDI: 1.16. ^{1}H NMR (400 MHz, DMSO-*d*$_6$, 22 °C): δ 13.05 (s, br, 20H, -COO*H*), 7.91 (m, 40H, -Ph*H*-), 7.12 (m, 40H, -Ph*H*-), 4.44 (m, 80H, -C*H*$_2$OCOO-), 3.50 (s, 909H, H of PEG), 1.34 (m, 60H, -CH$_3$).

Synthesis of carboxylic acid-functionalized polycarbonate Biotin-PEG-P(MTC-CH$_2$COOtBoc)$_{20}$: The cyclic monomer, MTC-tBAc, was synthesized as reported in the literature.[24] In a glovebox, Biotin-PEG-OH (M_n 10 kDa, 0.3 g, 0.03 mmol), MTC-tBAc (0.274 g, 1 mmol) and TU (18.5 mg, 0.05 mmol) were dissolved in 2 mL of dry DCM, followed by addition of DBU (7.47 μL, 0.05 mmol) and the reaction mixture was left to stir at room temperature for 2 h. Then, to quench the polymerization, benzoic acid (2-3 mg) was added in excess to the mixture. The resulting polymer was purified using size exclusion chromatography *via* a Sephadex LH-20 column, using THF as the eluent. After the solvent was removed, the residue was dried *in vacuo*, giving Biotin-PEG$_{10K}$-P(MTC-CH$_2$COOtBoc)$_{20}$ as a white solid (73% yield). ^{1}H NMR (400 MHz, DMSO-*d*$_6$, 22 °C): δ 4.57 (s, 40H, -C*H*$_2$COOtBoc), 4.27 (m, 80H, -C*H*$_2$OCOO-), 3.50 (s, 909H, H of PEG), 3.10 (m, 1H, biotin), 2.81 (dd, 1H, biotin), 2.06 (t, 2H, biotin), 1.39 (s, 180H, -C*H*$_3$ of tBoc), 1.22 (m, 60H, -C*H*$_3$).

Deprotection of Biotin-PEG-P(MTC-CH$_2$COOtBoc)$_{20}$: For removal of tBoc protecting groups, an acid-mediated deprotection strategy was adopted. Briefly, the above tBoc-protected polymer (0.3 g) was dissolved in dry DCM (2 mL) and trifluoroacetic acid (2 mL) and the reaction mixture was

left to stir at room temperature overnight. After the removal of solvent, the residue was re-dissolved in MeOH (2 mL) and precipitated in 20% hexane 80% Et_2O. After the precipitate was centrifuged and washed with Et_2O for 3 times, the solid obtained was dried *in vacuo*, giving pure Biotin-PEG-P(MTC-$CH_2COOH)_{20}$ as white solid (90% yield). Complete deprotection was confirmed by ^{1}H NMR analysis. ^{1}H NMR (400 MHz, DMSO-d_6, 22 °C): δ 13.14 (s, br, 20H, -COO*H*), 4.62 (s, 40H, -C*H*$_2$COOH), 4.27 (m, 80H, -C*H*$_2$OCOO-), 3.50 (s, 909H, H of PEG), 2.81 (dd, 1H, biotin), 2.06 (t, 2H, biotin), 1.21 (m, 60H, -C*H*$_3$).

Synthesis of carboxylic acid-functionalized polycarbonate PEG-P(MTC-$CH_2COOH)_{20}$: The polymer was synthesized by replacing the macro-initiator with mPEG (10 kDa) and using the same protocol described for the synthesis of Biotin-PEG-P(MTC-$CH_2COOH)_{20}$. Yield: 73%; ^{1}H NMR (400 MHz, DMSO-d_6, 22 °C): δ 13.14 (s, br, 20H, -COO*H*), 4.62 (s, 40H, -C*H*$_2$COOH), 4.27 (m, 80H, -C*H*$_2$OCOO-), 3.50 (s, 909H, H of PEG), 1.21 (m, 60H, -C*H*$_3$) (**Scheme S2**).

Polymer characterization: The molecular weights and polydispersity indices were determined by gel permeation chromatography and the chemical compositions were determined by ^{1}H NMR spectroscopy. The details of the instruments and parameters were the same as reported in the previous publication.[33]

Formation of nanocomplexes: For NP A, 27 mg/mL of anionic polymer dissolved in PBS was added dropwise into 15 mg/mL of pBu_20 in PBS. The mixture was vortexed for 30s. The mixture was left undisturbed at room temperature for 30 min before the unbounded polymers were removed using a ultracentrifugal filter (MWCO 10,000). The mixture was washed with water twice before it was lyophilized and stored under vacuum.

For NP B, 12 mg of anionic polymer was first dissolved in 1:1 mixture of dichloromethane and methanol. The organic solvents were removed via rotary evaporation to create a thin film on a glass vial. 20 mg of pBu_20 was dissolved in 1 mL of water and was added directly to hydrate the thin film. The mixture was immediately vortexed for 1 min, followed by 1 min sonication in a bath sonicator. The vortex and sonication procedures were repeated for another 2 times. The mixture was left undisturbed at room temperature for 30 min before the unbounded polymers were removed using a ultracentrifugal filter (MWCO 10,000). The mixture was washed with water twice before it was lyophilized and stored under vacuum.

Nanoparticle characterization: The particle size and zeta potential of the nanocomplexes were measured at 1.0 mg/mL in deionized (DI) water by dynamic light scattering (DLS) using Zetasizer 3000 HAS (Malvern Instrument Ltd.) and a He-Ne laser beam at 658 nm, with a scattering angle of 90 °. Each measurement was repeated 10 runs, and an average value was obtained from three measurements.

Transmission electron microscopy (TEM): The morphology of NP A_biotinPEG and NP B_biotinPEG was analyzed by TEM (Thermo Scientific Talos L120C electron microscope operated at an accelerated voltage of 120 k eV). Nanoparticles were resuspended in HPLC grade water at 2 mg/mL. Then, nanoparticles were mixed 1:1 volumetric ratio with phosphotungstic acid (0.2 w/v%) and incubated at room temperature for 30 min. A droplet (10 µL) of the mixture was added onto formvar/carbon-coated 200 mesh copper grid and incubated for 1 min before the excess solution was removed using a filter paper. The samples were air-dried overnight at room temperature prior to TEM observation.

Biotin availability: Pierce Biotin Quantitation Kit was used to quantitate the number of moles of biotin. 20 µL of HABA (4´-hydroxyazobenzene-2-carboxylic acid)/Avidin premix dissolved in

HPLC water was added to 160 µL of PBS in a microplate well. The absorbance of the mixture was measured at 500 nm (M1). Then 20 µL of the polymer solution or nanoparticles suspension was added to the well. The absorbance of the solution in the well at 500 nm (M2). The number of mmol of biotin per mmol of polymer was calculated as [(M1-M2)/(34000×0.5)]×10/[polymer concentration (mg/mL)/molecular weight of polymer (mg/mmol)] as recommended by the manufacturer. For the nanoparticles, the polymer concentration in the above equation was determined by multiplying the nanoparticle concentration (mg/mL) by the loading level.

Loading level of pBu_20 in the nanoparticles: Potassium hexacyanoferrate (5 mg/mL) and sodium nitroferricyanide(III) dihydrate (5 mg/mL) were dissolved in 1 M sodium hydroxide. 400 µL of this mixture was mixed with 300 µL of pBu_20 loaded nanoparticles dissolved in water (3 mg nanoparticles/mL).[25] After 30 min, the absorbance at 514 nm was measured. The loading level was calculated using a calibration curve prepared with pBu_20 in water (concentration range: 0.1875 – 3 mg/mL).

In vitro cytotoxicity: The cytotoxicity of pBu_20 and its nanoparticles against BT474, MCF7, MCF7/ADR cancer cell lines was measured using alamarBlue Cell Viability Reagent (ThermoFisher Scientific). Cells were seeded onto black 96-well plates at a density of 5,000 cells per well and incubated overnight. The media was replaced with fresh media containing the polymer or its nanoparticles at a range of concentrations (2 – 1,000 mg/L) and incubated for 24 h at 37 °C. After 24 h, the media was replaced with media containing alamarBlue reagent and further incubated for 8 h. The reduction of resazurin to resorufin was detected using a fluorescence microplate reader (excitation/emission at 540/590 nm).

Decomplexation of nanoparticles: NP A_biotinPEG and NP B_biotinPEG were dissolved in DI water to make up a final concentration of 1000 µg/mL. Separately, triton X-100 was dissolved in TE

buffer to make a 2.5% solution. After that, the respective nanoparticles suspension was added to the triton X-100 solution to make up a 10% nanoparticles suspension. The mixture was incubated at 37ºC and each sample was tested by DLS over a pre-determined period of time up to 24 h.

Quantitative analysis on the uptake of biotinylated nanoparticles via flow cytometry: Biotinylated NP_A and NP_B were first labelled with Alexa Fluor 488 respectively as described in an earlier publication.[23] BT474 cells were incubated with the respective nanoparticles (pBu_20: 30 µg/mL) for 2 h before being subjected to flow cytometry analysis. The count rates reflected the amount of nanoparticles uptaken by the cells over 2 h.

Intracellular distribution of pBu_20: pBu_20 was labelled with Alexa Fluor 488 as described in an earlier publication.[23] NP B were prepared with the labelled pBu_20 as described above. Cells were seeded onto 4-well chamber slides at a density of 125,000 cells per well and incubated overnight. The media was replaced with fresh media containing the labelled polymer or its nanoparticles at $0.5\times IC_{50}$ for 30 min. After 30 min, the polymer-containing media was removed and washed with PBS. The acidic organelles were labelled with LysoTracker™ Deep Red for 10 min at 37 °C. The cells were kept in the dark at room temperature and were imaged 2 h using a confocal microscope (Zeiss LSM 710, Germany) after the polymer was first added.

Analysis of cell apoptosis: BT474 or MCF7 cells were seeded overnight on 12 well plates at a density of 100,000 cells per well. The cells were then treated with pBu_20, NP B_mPEG10k or NP B_biotinPEG10k for 2 h. For the apoptosis positive control, cells were treated with paclitaxel (48 µg/mL). For the necrosis positive control, cells were treated with Triton X-100 (100 µg/mL). After 2 h, the cells were washed with PBS, lifted from the well plates, and treated according to the manufacturer's protocol for the Dead Cell Apoptosis Kit with Annexin V Alexa Fluor™ 488 & PI.

In vivo studies: Animal studies were performed according to protocols approved by the Singapore Biological Research Center's Institutional Animal Care and Use Committee (Protocol number 181374).

Pharmacokinetics and biodistribution of pBu_20 and its nanoparticles: The experiment was performed using a similar method as reported previously.[30] Balb/c mice (7 – 8 week old, n = 5) were injected with Alexa Fluor 750-conjugated pBu_20 complexed with the respective anionic polymers as described above as a single bolus into the tail vein (8 mg pBu_20/kg of mouse body weight in 100 µL of sterile PBS). Blood samples were collected in EDTA-coated vacutainers through cardiac puncture at 2, 5, 10, 30, 60, 120, 240, 480 and 1440 min. The plasma was immediately separated by centrifugation at 1000 × g for 10 min at 4°C. The fluorescence intensities of Alexa Fluor 740-conjugated pBu_20 in the plasma were measured on a clear bottom black 96-well plate at Ex/Em 749 nm/794 nm using a microplate reader (Tecan Spark^{TM} 10M, Switzerland). The concentrations of the polymer in the plasma were calculated using a calibration curve prepared with the same solution of Alexa Fluor 750-conjugated pBu_20 (concentration range: 0.5 – 500 µg mL^{-1}). Pharmacokinetic indices were calculated using PKSolver software.[34]

The kidneys, liver, lungs, spleen, heart and brain were also collected at each time point to determine the amount of pBu_20 in each organ. The organs were weighed and pulverized in 1 mL PBS using a tissue homogenizer. The concentrations of polymer in the individual organs were calculated using a calibration curve prepared by diluting Alexa Fluor 750-conjugated pBu_20 in the respective pulverized organ media.

Determination of median lethal dose (LD_{50}): We referred to the Up-and-Down-Procedure described in OECD Guidelines for the Testing of Chemicals (OECD 425). Balb/c mice were injected with pBu_20 and its nanoparticles via tail vein at doses of 15.8, 21.1, 28.1, 37.5, 50, 66.7,

88.9, and 118.5 mg/kg of mouse body weight. The survival rate of treated mice in each group was recorded over 7 days. The LD50 was estimated using the maximum likelihood method.[35]

In vivo anticancer efficacy: 9 week old female Balb/c nude mice (body weight: 16 – 20 g) were administered an estradiol pellet (0.72 mg/pellet, 60 day release, Innovative Research of America). BT474 cells in 1:1 mixture of RPMI/Geltrex™ LDEV-Free Reduced Growth Factor Basement Membrane Matrix (8 million/200 µL) were injected subcutaneously into the right flank of the mice. After 21 days, the mice bearing the BT-474 xenograft (100 – 150 mm^3) were divided into 5 groups (9 mice per group). Group 1: untreated mice as control, group 2 for treatment with pBu_20 without carrier, group 3 for NP B_mPEG, group 4 for NP B_biotinPEG. All formulations were administered to the mice via tail vein injection at day 0, 3, 7, 11 and 14 (pBu_20 dose: 8 or 20 mg/kg of mouse body weight). The mice were weighed, and the tumor size was measured using a Vernier caliper. The tumor volume (mm^3) was calculated using the formula: volume = (length × width × width)/2. One tumor from the NP B_biotin PEG group was excluded in the calculations because, based on Grubbs' Test, the tumor was considered an outlier.

21 days after the first injection, the mice were sacrificed, and the tumors were harvested. The tumors were weighed and the percentage tumor suppression was calculated using the formula: tumor suppression (%) = (average weight of tumors from the control group - average weight of tumors from treatment group)/(average weight of tumors from the control group) ×100%.

The tumors were fixed in a 10% neutral buffered formalin for 48 h, embedded in paraffin, sectioned, and stained according to the ApopTag® Peroxidase In Situ Apoptosis Detection Kit (Merck), which detects apoptotic cells in situ by labeling and detecting DNA strand breaks by TUNEL.

Statistical Analysis: For *in vitro* measurements, data were presented as mean ± standard deviation. For *in vivo* measurements, data are presented as mean ± standard error. All experiments were performed with at least three independent replicates. Student's t-tests, with two-tailed distribution and two-sample equal variance, were performed using Microsoft Excel. Differences were considered significant if p-values were less than 0.05.

Supporting Information

The Supporting Information is available free of charge.

Additional data on the median lethal dose of anticancer polymer pBu_20 and the nanoparticles, logarithmic partition coefficient, and the logarithmic acid dissociation constant, of the carboxylic acid and benzoic acid monomers, in vitro cytotoxicity of NP A, in vivo organ distribution of NP A and NP B, and stability of NP B in the presence of serum proteins.

Acknowledgement

This research was financially supported by the Bioprocessing Technology Institute and UIBR (Biomedical Research Council, Agency for Science, Technology and Research). J. Tay is grateful to Agency for Science, Technology and Research, Singapore for AGS PhD scholarship.

Conflict of Interest

The authors declare no conflict of interest.

References

[1] H. Sung, J. Ferlay, R. L. Siegel, M. Laversanne, I. Soerjomataram, A. Jemal, F. Bray, *CA Cancer J Clin* **2021**, 71, 209.
[2] D. J. Konieczkowski, C. M. Johannessen, L. A. Garraway, *Cancer Cell* **2018**, 33, 801.
[3] D. B. Longley, P. G. Johnston, *The Journal of Pathology* **2005**, 205, 275.
[4] S. Raguz, E. Yagüe, *British Journal of Cancer* **2008**, 99, 387.
[5] B. Li, S. W. Brady, X. Ma, S. Shen, Y. Zhang, Y. Li, K. Szlachta, L. Dong, Y. Liu, F. Yang, N. Wang, D. A. Flasch, M. A. Myers, H. L. Mulder, L. Ding, Y. Liu, L. Tian, K. Hagiwara, K. Xu, X. Zhou, E. Sioson, T. Wang, L. Yang, J. Zhao, H. Zhang, Y. Shao, H. Sun, L. Sun, J. Cai, H.-Y. Sun, T.-N. Lin, L. Du, H. Li, M. Rusch, M. N. Edmonson, J. Easton, X. Zhu, J. Zhang, C. Cheng, B. J. Raphael, J. Tang, J. R. Downing, L. B. Alexandrov, B.-B. S. Zhou, C.-H. Pui, J. J. Yang, J. Zhang, *Blood* **2020**, 135, 41.
[6] A. C. Anselmo, S. Mitragotri, *Bioeng Transl Med* **2019**, 4, e10143.
[7] J. Tan, J. Tay, J. Hedrick, Y. Y. Yang, *Biomaterials* **2020**, 252, 120078.
[8] S. Riedl, D. Zweytick, K. Lohner, *Chem Phys Lipids* **2011**, 164, 766.
[9] a)J. Zhao, Z. Dong, H. Cui, H. Jin, C. Wang, *ACS Appl Mater Interfaces* **2018**, 10, 42058; b)F. Qi, Y. Qian, N. Shao, R. Zhou, S. Zhang, Z. Lu, M. Zhou, J. Xie, T. Wei, Q. Yu, R. Liu, *ACS Appl Mater Interfaces* **2019**, 11, 18907.
[10] N. H. Park, W. Cheng, F. Lai, C. Yang, P. Florez de Sessions, B. Periaswamy, C. Wenhan Chu, S. Bianco, S. Liu, S. Venkataraman, Q. Chen, Y. Y. Yang, J. L. Hedrick, *J Am Chem Soc* **2018**, 140, 4244.
[11] M. R. Felicio, O. N. Silva, S. Goncalves, N. C. Santos, O. L. Franco, *Front Chem* **2017**, 5, 5.
[12] C. Allolio, A. Magarkar, P. Jurkiewicz, K. Baxova, M. Javanainen, P. E. Mason, R. Sachl, M. Cebecauer, M. Hof, D. Horinek, V. Heinz, R. Rachel, C. M. Ziegler, A. Schrofel, P. Jungwirth, *Proc Natl Acad Sci U S A* **2018**, 115, 11923.
[13] a)G. Zhong, C. Yang, S. Liu, Y. Zheng, W. Lou, J. Y. Teo, C. Bao, W. Cheng, J. P. K. Tan, S. Gao, N. Park, S. Venkataraman, Y. Huang, M. H. Tan, X. Wang, J. L. Hedrick, W. Fan, Y. Y. Yang, *Biomaterials* **2019**, 199, 76; b)J. Tay, Y. Zhao, J. L. Hedrick, Y. Y. Yang, *Theranostics* **2021**, 11, 8977.
[14] M. A. Warso, J. M. Richards, D. Mehta, K. Christov, C. Schaeffer, L. Rae Bressler, T. Yamada, D. Majumdar, S. A. Kennedy, C. W. Beattie, T. K. Das Gupta, *Br J Cancer* **2013**, 108, 1061.
[15] a)Y. F. Chen, A. L. Shiau, S. J. Chang, N. S. Fan, C. T. Wang, C. L. Wu, J. S. Jan, *Acta Biomater* **2017**, 55, 283; b)H. Takahashi, K. Yumoto, K. Yasuhara, E. T. Nadres, Y. Kikuchi, L. Buttitta, R. S. Taichman, K. Kuroda, *Sci Rep* **2019**, 9, 1096.
[16] a)F. Fan, J.-G. Piao, Y. Zhao, L. Jin, M. Li, Y. Wang, L. Yang, *ACS Applied Bio Materials* **2020**, 3, 1267; b)F. Fan, L. Jin, L. Yang, *ACS Appl Mater Interfaces* **2021**, 13, 12824.
[17] A. D. Vadlapudi, R. K. Vadlapatla, A. K. Mitra, *Curr Drug Targets* **2012**, 13, 994.
[18] a)G. Russell-Jones, K. McTavish, J. McEwan, J. Rice, D. Nowotnik, *Journal of Inorganic Biochemistry* **2004**, 98, 1625; b)W. X. Ren, J. Han, S. Uhm, Y. J. Jang, C. Kang, J.-H. Kim, J. S. Kim, *Chemical Communications* **2015**, 51, 10403.
[19] a)A. B. Attia, C. Yang, J. P. Tan, S. Gao, D. F. Williams, J. L. Hedrick, Y. Y. Yang, *Biomaterials* **2013**, 34, 3132; b)X. Ke, D. J. Coady, C. Yang, A. C. Engler, J. L. Hedrick, Y. Y. Yang, *Polymer Chemistry* **2014**, 5; c)A. L. Lee, S. Venkataraman, S. B. Sirat, S. Gao, J. L. Hedrick,

Y. Y. Yang, *Biomaterials* **2012**, 33, 1921; d)J. Leong, W. Chin, X. Ke, S. Gao, H. Kong, J. L. Hedrick, Y. Y. Yang, *Nanomedicine* **2018**, 14, 2666; e)J. Y. Teo, W. Chin, X. Ke, S. Gao, S. Liu, W. Cheng, J. L. Hedrick, Y. Y. Yang, *Nanomedicine* **2017**, 13, 431.
[20] a)Y. Li, C. Yang, M. Khan, S. Liu, J. L. Hedrick, Y. Y. Yang, P. L. Ee, *Biomaterials* **2012**, 33, 6533; b)Z. Y. Ong, K. Fukushima, D. J. Coady, Y. Y. Yang, P. L. Ee, J. L. Hedrick, *J Control Release* **2011**, 152, 120; c)Z. Y. Ong, C. Yang, W. Cheng, Z. X. Voo, W. Chin, J. L. Hedrick, Y. Y. Yang, *Acta Biomater* **2017**, 54, 201.
[21] E. W. P. Tan, J. L. Hedrick, P. L. Arrechea, T. Erdmann, V. Kiyek, S. Lottier, Y. Y. Yang, N. H. Park, *Macromolecules* **2021**, 54, 1767.
[22] A. L. Z. Lee, Z. X. Voo, W. Chin, R. J. Ono, C. Yang, S. Gao, J. L. Hedrick, Y. Y. Yang, *ACS Applied Materials & Interfaces* **2018**, 10, 13274.
[23] W. Chin, G. Zhong, Q. Pu, C. Yang, W. Lou, P. F. De Sessions, B. Periaswamy, A. Lee, Z. C. Liang, X. Ding, S. Gao, C. W. Chu, S. Bianco, C. Bao, Y. W. Tong, W. Fan, M. Wu, J. L. Hedrick, Y. Y. Yang, *Nat Commun* **2018**, 9, 917.
[24] A. Bossion, G. O. Jones, D. Taton, D. Mecerreyes, J. L. Hedrick, Z. Y. Ong, Y. Y. Yang, H. Sardon, *Langmuir* **2017**, 33, 1959.
[25] a)C. J. Weber, *Journal of Biological Chemistry* **1928**, 78, 465; b)J. L. Choi, J. K. Tan, D. L. Sellers, H. Wei, P. J. Horner, S. H. Pun, *Biomaterials* **2015**, 54, 87.
[26] Z. Zhou, Y. Shen, J. Tang, M. Fan, E. A. Van Kirk, W. J. Murdoch, M. Radosz, *Advanced Functional Materials* **2009**, 19, 3580.
[27] a)W. Shen, Y. Zhang, P. Wan, L. An, P. Zhang, C. Xiao, X. Chen, *Advanced Materials* **2020**, 32, 2001108; b)Y. Wang, W. Shen, S. Liu, G. Zhu, X. Meng, K. Mao, J. Wang, Y.-G. Yang, C. Xiao, T. Sun, *Macromolecular Bioscience* **2021**, 21, 2100171; c)N. Shao, L. Yuan, P. Ma, M. Zhou, X. Xiao, Z. Cong, Y. Wu, G. Xiao, J. Fei, R. Liu, *Journal of the American Chemical Society* **2022**, 144, 7283.
[28] E. I. Geihe, C. B. Cooley, J. R. Simon, M. K. Kiesewetter, J. A. Edward, R. P. Hickerson, R. L. Kaspar, J. L. Hedrick, R. M. Waymouth, P. A. Wender, *Proc Natl Acad Sci U S A* **2012**, 109, 13171.
[29] F. Wang, Y.-C. Wang, S. Dou, M.-H. Xiong, T.-M. Sun, J. Wang, *ACS Nano* **2011**, 5, 3679.
[30] C. Yang, W. Lou, G. Zhong, A. Lee, J. Leong, W. Chin, B. Ding, C. Bao, J. P. K. Tan, Q. Pu, S. Gao, L. Xu, L. Y. Hsu, M. Wu, J. L. Hedrick, W. Fan, Y. Y. Yang, *Acta Biomater* **2019**, 94, 268.
[31] R. C. Pratt, F. Nederberg, R. M. Waymouth, J. L. Hedrick, *Chemical Communications* **2008**, 114.
[32] R. C. Pratt, B. G. G. Lohmeijer, D. A. Long, P. N. P. Lundberg, A. P. Dove, H. B. Li, C. G. Wade, R. M. Waymouth, J. L. Hedrick, *Macromolecules* **2006**, 39, 7863.
[33] A. L. Z. Lee, C. Yang, S. Gao, Y. Wang, J. L. Hedrick, Y. Y. Yang, *ACS Appl Mater Interfaces* **2020**, 12, 52285.
[34] Y. Zhang, M. Huo, J. Zhou, S. Xie, *Comput Methods Programs Biomed* **2010**, 99, 306.
[35] OECD, *Test No. 425: Acute Oral Toxicity: Up-and-Down Procedure*, **2008**.

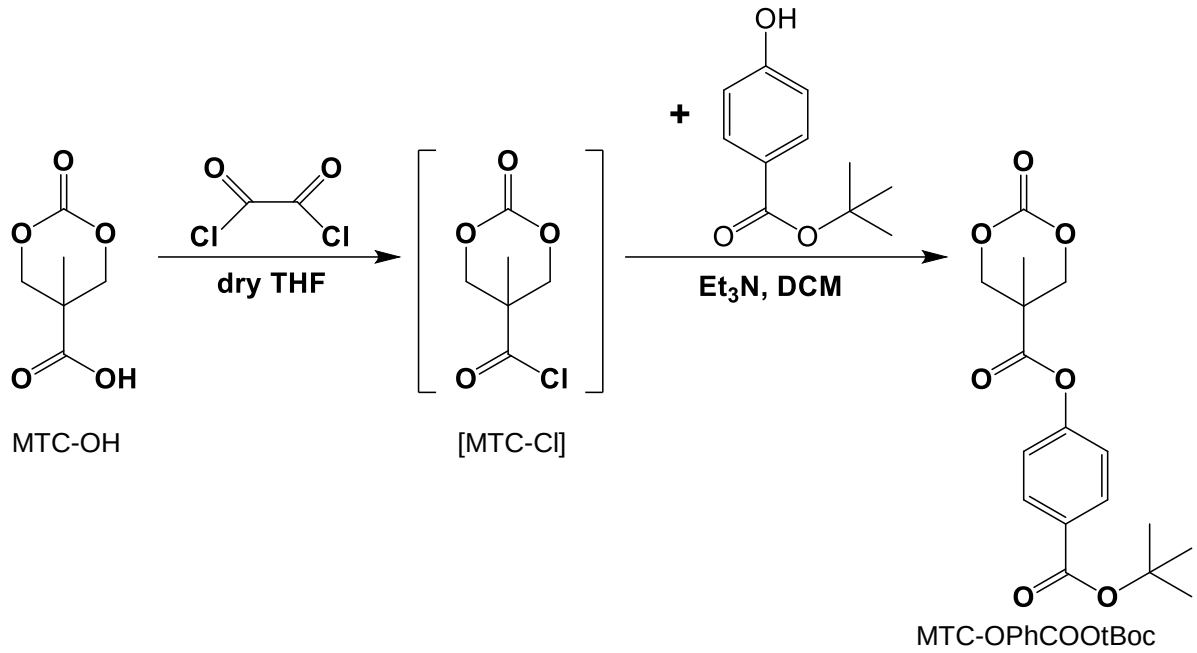

Scheme S1. Chemical structure and synthetic procedures of MTC-OPhCOOtBoc.

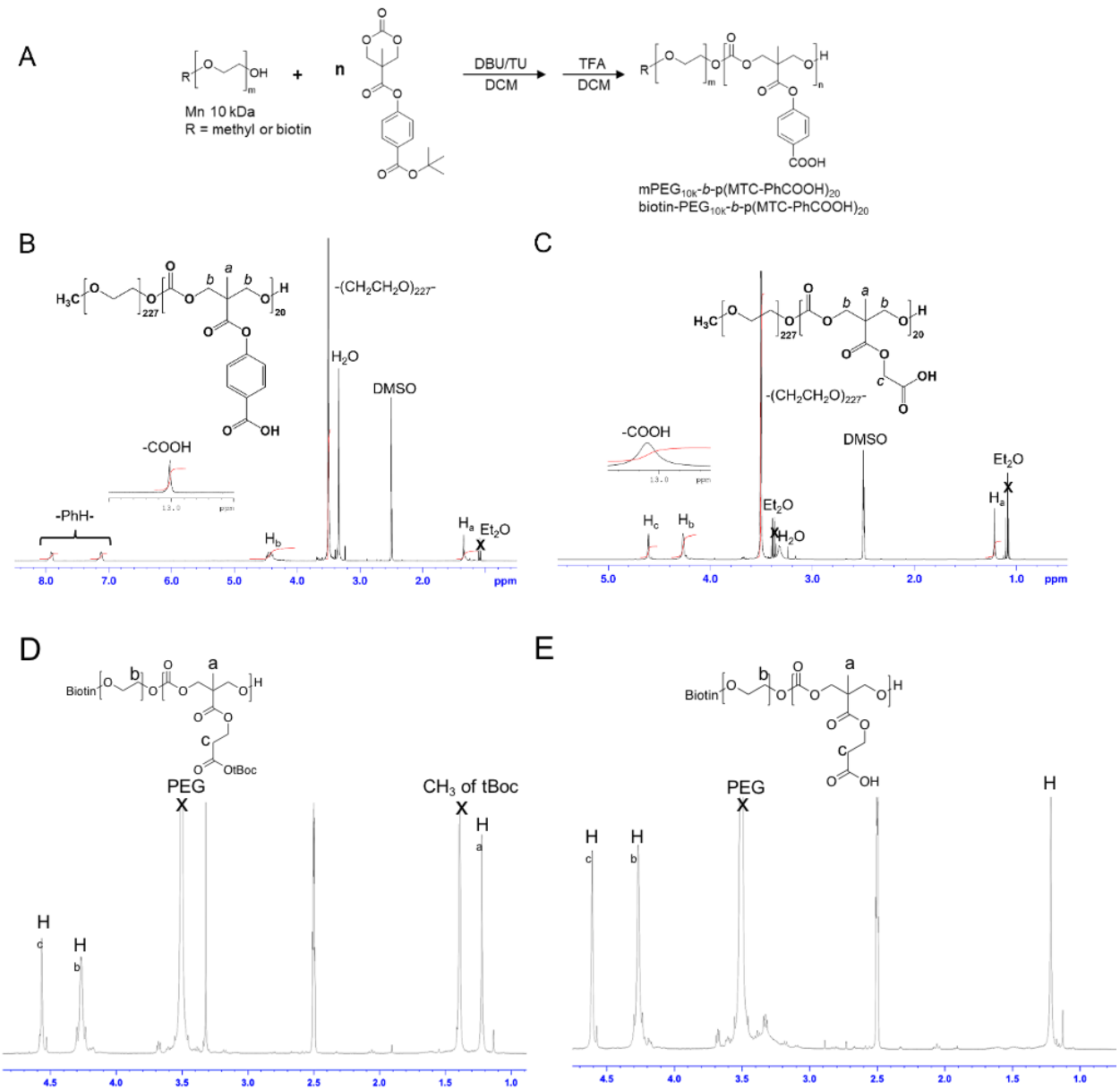

Scheme S2. (A) Synthetic procedures of benzoic acid-functionalized polycarbonates and ^{1}H NMR spectrums of (B) mPEG$_{10K}$-P(MTC-PhCOOH)$_{20}$, (C) mPEG$_{10K}$-P(MTC-CH$_2$COOH)$_{20,}$ (D) biotin-PEG-p(MTC-CH$_2$COOtBoc)$_{20}$ and (E) biotin-PEG-p(MTC-CH$_2$COOH)$_{20}$ in DMSO-d_6.

Table S1. Plasma concentrations of pBu_20 in mice at various timepoints after injection with NP A_mPEG.

Time (min)	Concentrations of AF750_labelled pBu_20 (μg/mL)				
	Replicate 1	**Replicate 2**	**Replicate 3**	**Replicate 4**	**Replicate 5**
2	123.417	115.452	74.654	82.338	73.380
5	87.042	68.189	84.943	65.603	73.999
10	29.753	27.129	30.371	27.129	27.673
30	14.854	17.066	14.011	15.866	16.447
60	9.063	5.751	7.698	5.858	9.477
120	5.168	5.536	5.321	6.165	5.674
240	2.592	1.672	1.488	1.810	1.779
480	1.227	0.736	0.491	0.659	0.905
1440	0.307	0.322	0.230	0.230	0.307
T1/2 (min)	411.8706	565.2399	265.9278	449.7463	506.5718
Average (min)	440		S.D.	113	

Table S2. Plasma concentrations of pBu_20 in mice at various timepoints after injection with NP A_biotin PEG.

Time (min)	Concentrations of AF750_labelled pBu_20 (μg/mL)				
	Replicate 1	**Replicate 2**	**Replicate 3**	**Replicate 4**	**Replicate 5**
2	62.651	51.808	33.375	44.034	33.763
5	32.164	32.932	37.285	38.247	25.037
10	19.898	22.375	25.703	22.042	18.742
30	12.031	10.875	9.156	7.908	8.897
60	3.229	3.466	3.675	4.984	5.959
120	1.076	1.076	0.644	0.547	0.498
240	0.223	0.275	0.339	0.368	0.264
480	0.099	0.108	0.075	0.151	0.075
1440	0.047	0.061	0.052	0.080	0.047
T1/2 (min)	604.7143	651.3912	417.4984	523.9666	446.4512
Average (min)	529		S.D.	100	

Table S3. Plasma concentrations of pBu_20 in mice at various timepoints after injection with NP B_mPEG.

Time (min)	Concentrations of AF750_labelled pBu_20 (μg/mL)				
	Replicate 1	**Replicate 2**	**Replicate 3**	**Replicate 4**	**Replicate 5**
2	22.70	26.92	22.95	20.35	15.79
5	14.98	14.02	13.88	13.47	11.02
10	9.72	8.91	7.70	7.28	6.82
30	5.71	4.74	4.69	4.04	3.29
60	2.71	2.08	2.07	2.02	1.83
120	1.16	1.06	0.91	0.90	0.89
240	0.181	0.179	0.149	0.133	0.127
480	0.092	0.048	0.046	0.0437	0.0437
1440	0.020	0.0153	0.0153	0.013	0.011
T1/2 (min)	389.2	383.9	412.5	398.6	370.4
Average (min)	390.9		S.D.	15.8	

Table S4. Plasma concentrations of pBu_20 in mice at various timepoints after injection with NP B_biotin PEG.

Time (min)	Concentrations of AF750_labelled pBu_20 (μg/mL)				
	Replicate 1	**Replicate 2**	**Replicate 3**	**Replicate 4**	**Replicate 5**
2	22.5	22.3	26.2	22.4	N.D.
5	10.5	8.7	9.1	10.0	12.4
10	3.5	5.3	4.3	4.9	3.4
30	19.5	18.5	13.7	13.9	17.2
60	3.0	2.9	2.6	2.4	2.2
120	1.0	1.1	1.3	0.9	0.8
240	0.15	0.27	0.22	0.50	0.28
480	0.04	0.06	0.04	0.05	0.20
1440	0.01	0.01	0.02	0.02	0.01
T1/2 (min)	340.7	302.1	161.7	215.4	239.9
Average (min)	252.0		S.D.	70.8	

Table S5. Median lethal dose (LD_{50}) when pBu_20 or its nanoparticles were administered to mice through tail vein injection.

Polymer/Nanoparticle	LD_{50} (mg/kg)
pBu_20	27
NP A_mPEG	>175*
NP A_biotin PEG	>175*
NP B_mPEG	174
NP B_biotin PEG	77

*Nanoparticles could not be resuspended at concentrations higher than 175 mg pBu_20 /kg

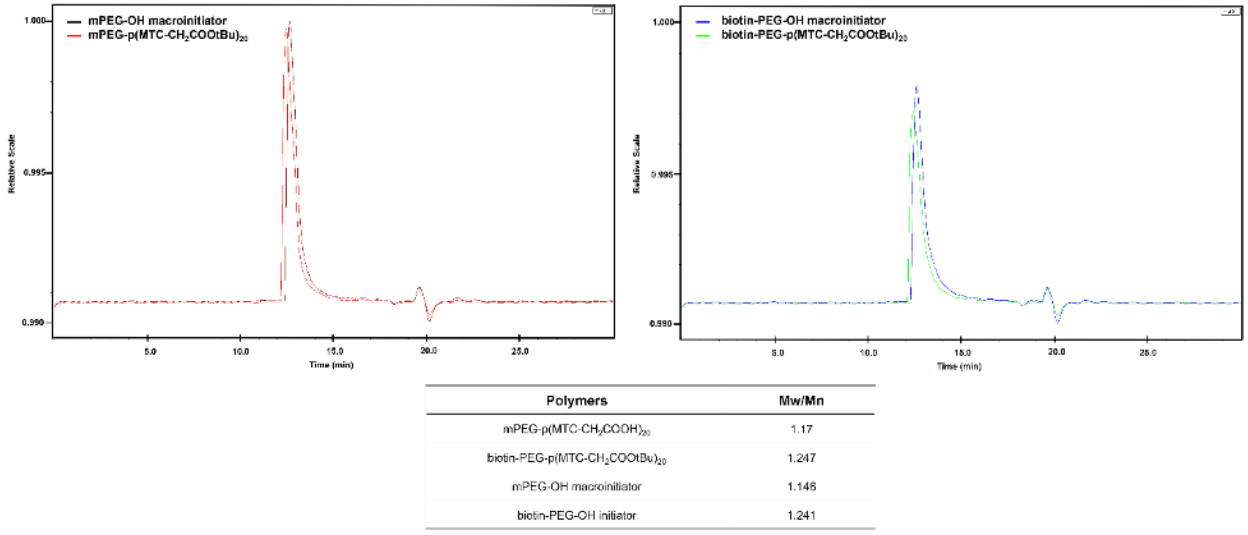

Polymers	Mw/Mn
mPEG-p(MTC-CH_2COOH)$_{20}$	1.17
biotin-PEG-p(MTC-CH_2COOtBu)$_{20}$	1.247
mPEG-OH macroinitiator	1.146
biotin-PEG-OH initiator	1.241

Figure S1. GPC (gel permeation chromatography) chromatograms of mPEG-p(MTC-CH_2COOtBu)$_{20}$ and biotin-PEG-p(MTC-CH_2COOtBu)$_{20}$ indicated that the polymers exhibited narrow molecular weight distributions with low polydispersity indices of 1.17 and 1.25, respectively.

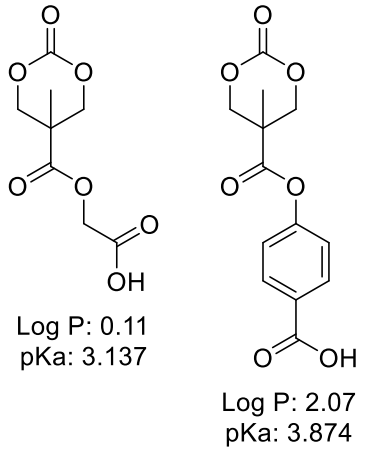

Figure S2. Logarithmic partition coefficient, Log P, and the logarithmic acid dissociation constant, pKa of the carboxylic acid and benzoic acid monomers.

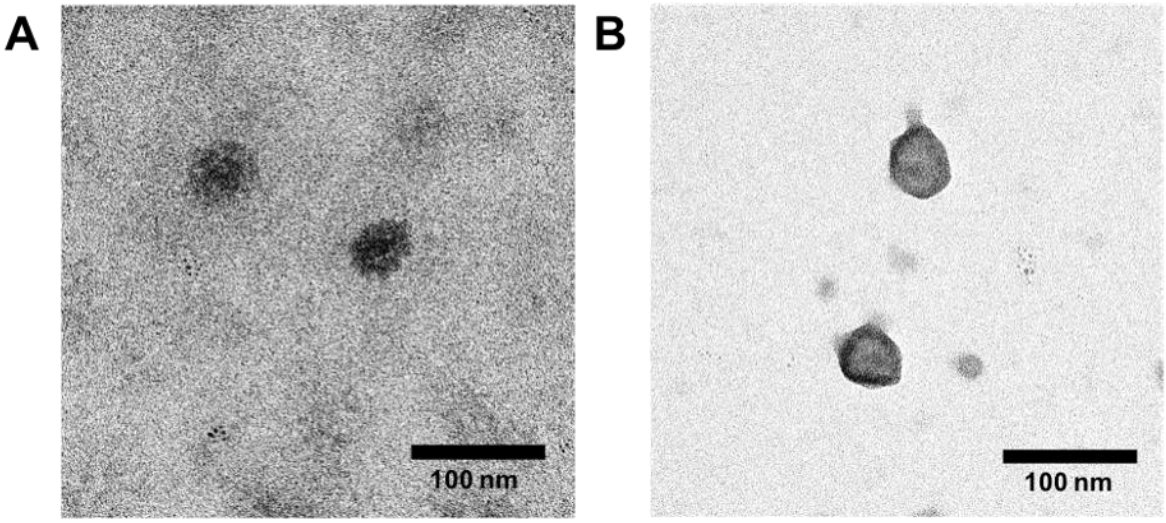

Figure S3. TEM images of (A) NP A_biotinPEG and (B) NP B_biotinPEG. The nanoparticles formed are spherical in shape.

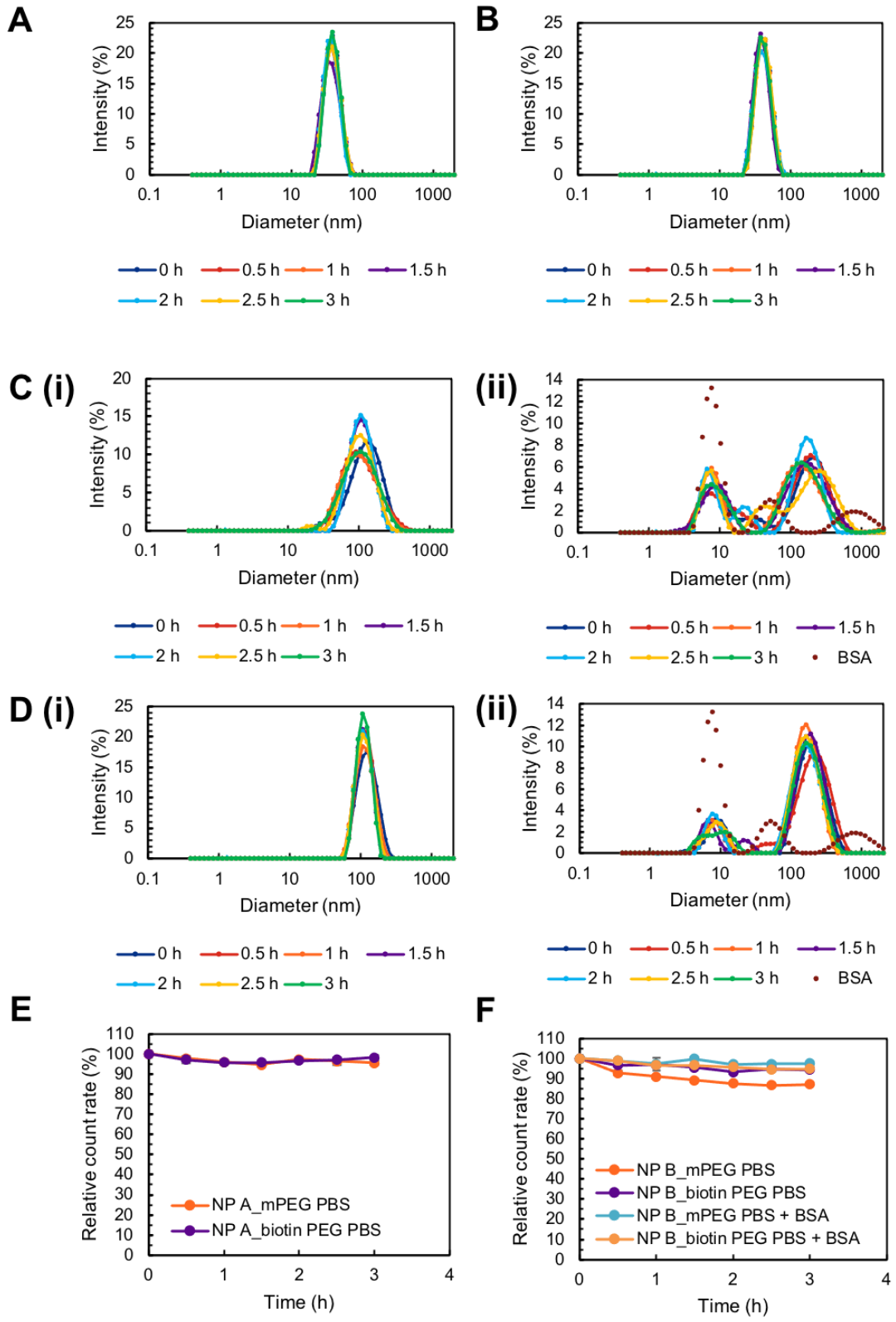

Figure S4. Hydrodynamic diameter measurements over 3 h. (A) NP A_mPEG and (B) NP A_biotin PEG in PBS. (C) NP B_mPEG and (D) NP B_biotin PEG in (i) PBS or (ii) BSA-containing PBS (80 g/L). (E) Relative count rates of NP_A and (F) NP_B over 3 h.

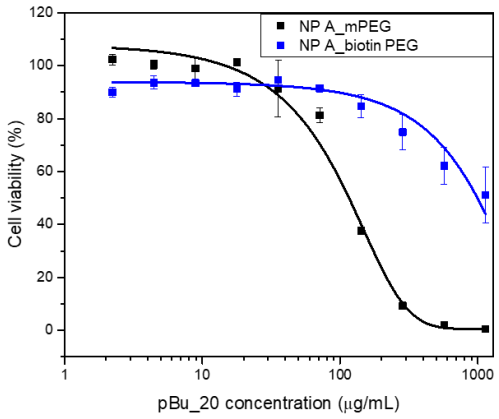

	IC50 (µg/mL)
pBu_20	13.6 ± 0.6
NP A_mPEG	135 ± 4
NP A_biotin PEG	1002 ± 17

Figure S5. *In vitro* cytotoxicity of pBu_20 and its nanoparticles against BT474 breast cancer cell line.

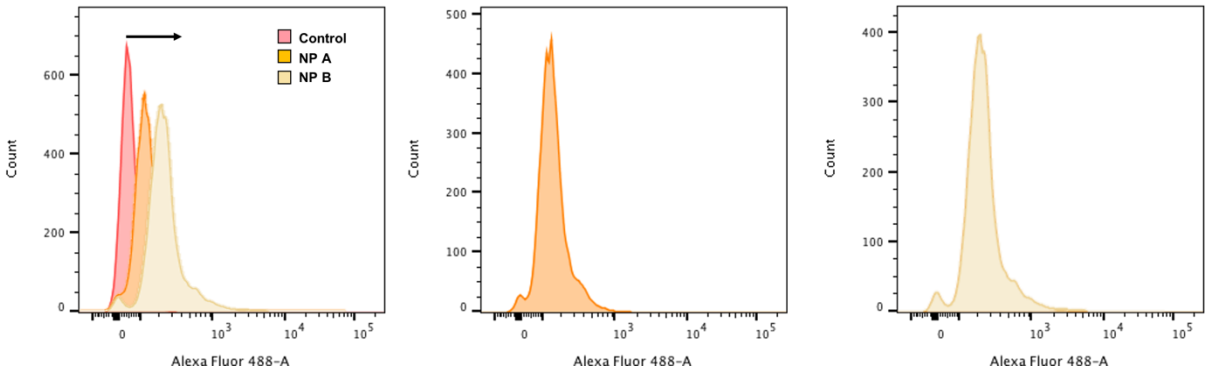

Figure S6. Uptake of AF488-labelled NP A and NP B (pBu_20: 30 µg/mL) by BT474 cells after 2 h of incubation.

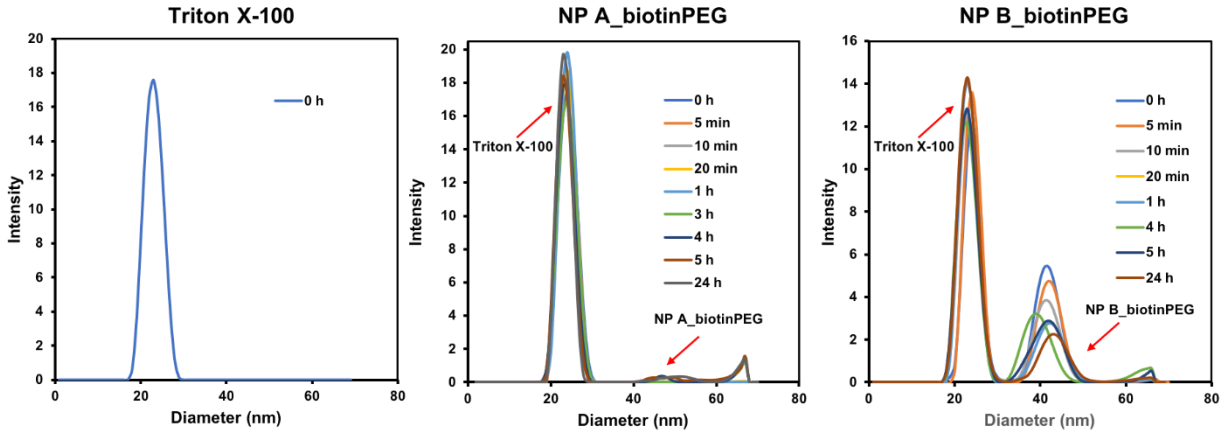

Figure S7. Intensity of NP A_biotinPEG and NP B_biotinPEG suspension in DI water, measured by dynamic light scattering at 500 nm in the presence of Triton X-100 at 2.5% to study dissociation of NP A_biotinPEG and NP B_biotinPEG.

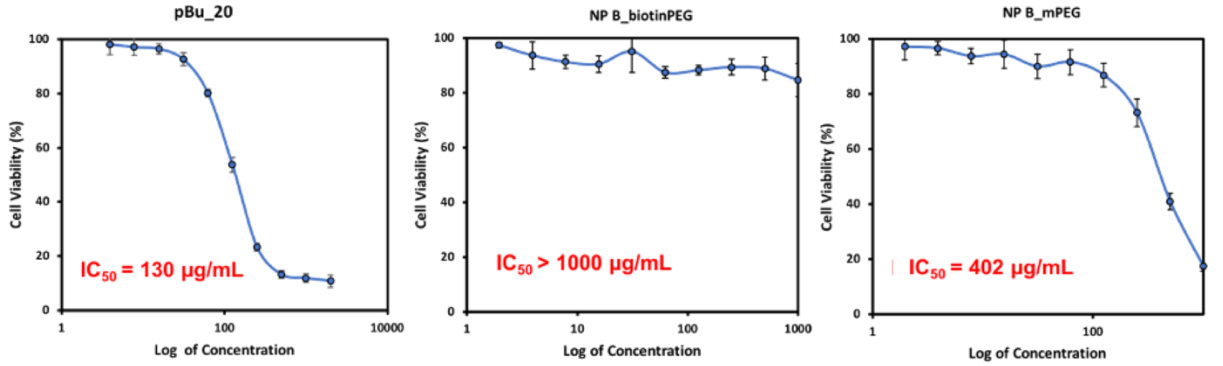

Samples	IC_{50} of BT474 (no endocytosis blocker) 24 h	IC_{50} of BT474 (no endocytosis blocker) 2 h	IC_{50} of BT474 (with endocytosis blocker) 2 h
Free polymer	13.6	180.0	130.0
NP B_biotinPEG	25.0	40.0	> 1000
NP B_mPEG	34.4	120.0	402.0

Figure S8. BT-474 cells were pre-treated with 5 µg/mL of the endocytosis blocker chlorpromazine. The IC_{50} values of pBu_20, NP B_mPEG and NP B_biotinPEG obtained were 130.0 µg/mL, 402.0 µg/mL and > 1000 µg/mL, respectively. The IC_{50} value of the pure anticancer polymer pBu_20 did not change significantly in the presence of chlorpromazine (IC_{50}: 130 *vs.* 180 µg/mL). However, the IC_{50} values of NP B_mPEG and NP B_biotinPEG obtained from chlorpromazine pre-treated cells were much higher than the IC_{50} values obtained without chlorpromazine pre-treatment (120.0 *vs.* 402.0 µg/mL; >1000 *vs.* 40.0 µg/mL). Incubation time: 2 h.

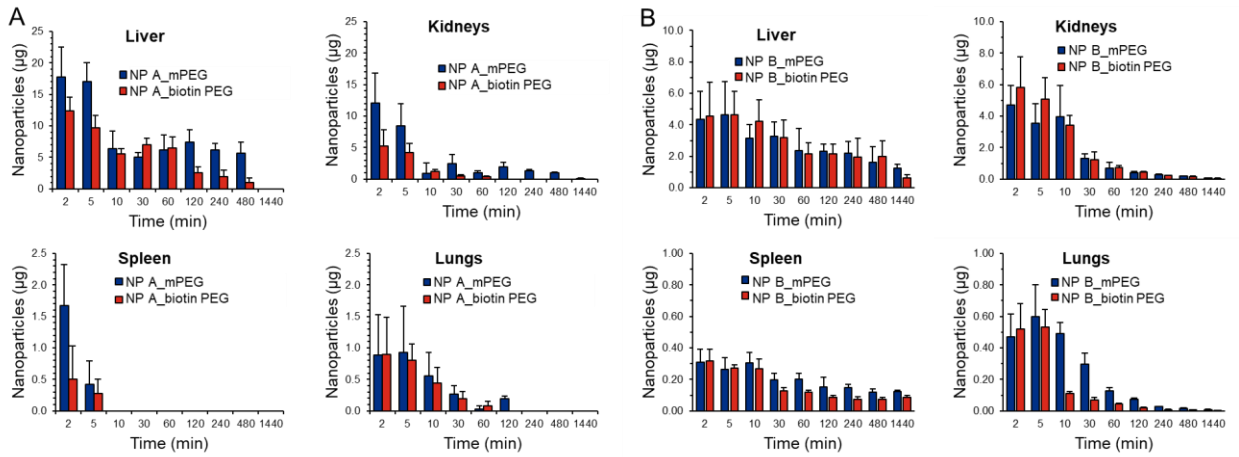

Figure S9. Organ distribution of Nanoparticles (A) and (B) over 24 h after one injection *via* the tail vein.